Geoscientific
Model Development

Peatland-VU-NUCOM (PVN 1.0): using dynamic plant functional types to model peatland vegetation, CH$_4$, and CO$_2$ emissions

Tanya J. R. Lippmann[1], **Ype van der Velde**[1], **Monique M. P. D. Heijmans**[2], **Han Dolman**[3,4], **Dimmie M. D. Hendriks**[5], **and Ko van Huissteden**[1,6]

[1]Department of Earth Sciences, Vrije Universiteit, Amsterdam, the Netherlands
[2]Department of Environmental Sciences, Wageningen University and Research, Wageningen, the Netherlands
[3]Royal Netherlands Institute for Sea Research, Texel, the Netherlands
[4]Netherlands Earth System Science Center, Utrecht University, Utrecht, the Netherlands
[5]Department of Soil and Groundwater Systems, Deltares Research Institute, Utrecht, the Netherlands
[6]VOF Kytalyk Carbon Cycle Research, Epse, the Netherlands

Correspondence: Tanya J. R. Lippmann (t.j.r.lippmann@vu.nl)

Abstract. Despite covering only 3 % of the planet's land surface, peatlands store 30 % of the planet's terrestrial carbon. The net greenhouse gas (GHG) emissions from peatlands depend on many factors but primarily soil temperature, vegetation composition, water level and drainage, and land management. However, many peatland models rely on water levels to estimate CH$_4$ exchange, neglecting to consider the role of CH$_4$ transported to the atmosphere by vegetation. To assess the impact of vegetation on the GHG fluxes of peatlands, we have developed a new model, Peatland-VU-NUCOM (PVN). The PVN model is a site-specific peatland CH$_4$ and CO$_2$ emissions model, able to reproduce vegetation dynamics. To represent dynamic vegetation, we have introduced plant functional types and competition, adapted from the NUCOM-BOG model, into the framework of the Peatland-VU model, a peatland GHG emissions model. The new PVN model includes plant competition, CH$_4$ diffusion, ebullition, root, shoot, litter, exudate production, belowground decomposition, and aboveground moss development under changing water levels and climatic conditions.

Here, we present the PVN model structure and explore the model's sensitivity to environmental input data and the introduction of the new vegetation competition schemes. We evaluate the model against observed chamber data collected at two peatland sites in the Netherlands to show that the model is able to reproduce realistic plant biomass fractions and daily CH$_4$ and CO$_2$ fluxes. We find that daily air temper-
ature, water level, harvest frequency and height, and vegetation composition drive CH$_4$ and CO$_2$ emissions. We find that this process-based model is suitable to be used to simulate peatland vegetation dynamics and CH$_4$ and CO$_2$ emissions.

1 Introduction

Despite covering only 3 % of the planet's land surface, peatlands store 30 % (644 GtC) of the planet's terrestrial carbon (Yu et al., 2010). The present-day global radiative effect of peatlands on the climate is estimated to be between -0.2 and $-0.5\,\mathrm{W\,m^{-2}}$ (i.e. a net cooling) (Frolking and Roulet, 2007) in comparison to a radiative forcing of $+2.43\,\mathrm{W\,m^{-2}}$ due to anthropogenic greenhouse gas (GHG) emissions since pre-industrial times (WGI, 2021). Future changes to the climate will impact the carbon sequestration capacity of peatlands; however, the net effect of climate change on peatlands is not yet understood (Loisel et al., 2021). Research indicates that some peatlands will form a positive feedback (Dorrepaal et al., 2009), whilst others will form a neutral (Saleska et al., 2002) or negative feedback to warming of the global climate system (Melillo et al., 2002; Lafleur et al., 2003), and the net effect of these complex responses is not yet known. The net warming effect of peatlands on the global climate system, and particularly the potential to both emit and draw-

down CO_2 and CH_4, means that peatlands have a complex and multifaceted relationship with the global climate system.

The net GHG emissions from peatlands depends on many factors but primarily vegetation composition, land management, ground water level and drainage, and soil temperature (Dorrepaal et al., 2009; Tiemeyer et al., 2016). Rewetting drained peatlands is one strategy proposed to combat enhanced CO_2 emissions from peatlands, but this has been documented to both enhance and reduce GHG emissions (e.g. Günther et al., 2020; Boonman et al., 2022) with the majority of studies concluding that rewetting leads to enhanced CH_4 and net GHG emissions (Harpenslager et al., 2015; Knox et al., 2015). Field studies have shown that vegetation restoration in combination with rewetting may reduce GHG emissions (Graf and Rochefort, 2009; Mazzola et al., 2022). Vegetation impacts the net GHG emissions in peatlands by directly influencing the net primary production and organic matter available for decomposition and indirectly and by influencing the substrates available for microbial metabolisation in the soil column (Bansal et al., 2020; Bridgham et al., 2013).

While the effects of the groundwater table on peatland GHG emissions are extensively described (Evans et al., 2021), the impacts of plant type and plant community composition on GHG emissions are less understood (Malmer et al., 2003). Changes in vegetation composition have been observed in long-running water table manipulation experiments (Peltoniemi et al., 2009; Strack et al., 2006). Generally, sedges and mosses establish during wetter conditions, and shrubs and trees develop during drier conditions, with enhanced *Sphagnum* growth outcompeting shrubs during warming experiments (Dorrepaal et al., 2006). Belowground, changes in vegetation have been accompanied by changes in bacterial and fungal biomass (Jaatinen et al., 2008) and methanogenic and methanotrophic community diversity (Yrjälä et al., 2011; Lippmann et al., 2021). Changes to CO_2 (NPP) have been observed following changes in plant community composition, further impacting root exudation (Ballantyne et al., 2014). Root exudates are a diverse group of organic compounds secreted by plant roots into the nearby soil. The composition and quality of root exudates varies between plant types, influencing microbial community composition and function and CO_2 (Crow and Wieder, 2005) and CH_4 fluxes (Schipper and Reddy, 1996). Plant growth, root exudation, and decomposition of organic matter happen at rates that differ depending on plant type (Dorrepaal et al., 2007). *Sphagnum* is a primary contributor to the carbon sequestration in many peatlands and decomposes 3 times slower than most vascular plants (Graf and Rochefort, 2009). Spatial variation in the rate of vegetation growth and decomposition, particularly for bryophyte species, leads to the creation of microforms, such as hummocks, hollows, and lawns, which, in turn, impact the water level relative to the surface and spatially variable fluxes (Waddington and Roulet, 2000). Differences in vegetation composition within the same site and

with the same water levels have been observed to lead to differences in CH_4 fluxes (Bubier, 2016; Jackowicz-Korczyński et al., 2010). To understand the role of vegetation emissions' feedbacks during peatland restoration efforts, vegetation must thus be treated as a dynamic interactive element of the peatland ecosystem.

Plants with common ecosystem functions or structures can be represented with common model algorithms or parameters in a vegetation model when grouped as plant functional types (PFTs) (Wullschleger et al., 2014). Plant functional types have been found to explain uncertainties in GHG emissions from wetlands in response to warming in a meta-analysis of wetlands exposed to warming (Bao et al., 2023). Dynamic (rather than static) PFTs simulate the inter-seasonal growing and dying of plants that, over a number of years, lead to vegetation succession and are critical to reliably assess the impacts of climate and environmental change on peatland ecosystems (Box et al., 2019). Shifts in community composition lead to feedbacks between species and other environmental parameters such as soil moisture, bulk density, soil organic matter (SOM) content, gas conduit function, rate of growth, rate of decomposition, microbial mineralisation, and aerobic decomposition (De Boeck et al., 2011). Dynamic plant representation is critical to reliably simulate vegetation–environmental feedbacks in models (Toet et al., 2006); therefore, the inclusion of dynamic vegetation classes is critical to reliably estimate C, CO_2, and CH_4 emissions from peatlands during periods of environmental change (Li et al., 2016; Laine et al., 2022).

Many peatland carbon cycle models have been developed over the preceding decades. The Wetland and Wetland CH_4 Inter-comparison of Models Project (WETCHIMP) evaluated the ability of a variety of models to simulate large-scale wetland characteristics and corresponding CH_4 emissions (Melton et al., 2013; Wania et al., 2013). Peatland modelling efforts have made significant advancements to simulate CH_4 fluxes by including CH_4-specific processes such as CH_4 plant transport and ebullition. However, many models rely on CO_2 fluxes or surface water levels as indicators of CH_4 exchange (Metzger et al., 2015), restricting their capacity to assess feedbacks between environmental change and the peatland CH_4 cycle. There exist two pre-existing models that simulate dynamic vegetation, CO_2, and CH_4 cycling in peatlands (i.e. PEATBOG (Wu et al., 2016) and LPJ-WHyMe (Wania et al., 2010)), thereby limiting the ability of the modelling community to assess model mechanistic processes. The functionality and scope of current models that simulate peatlands and include either dynamic or static vegetation are compared in Table S1 in the Supplement. The PEATBOG model simulates three PFTs – moss, shrubs, and graminoids – at the Mer Bleue bog site and represents a comprehensive array of peatland processes, including the nitrogen cycle and dissolved gases (carbon, CO_2, and CH_4). LPJ-WHyMe, like its parent model, LPJ-WHy (Sitch et al., 2003; Gerten et al., 2004), includes permafrost
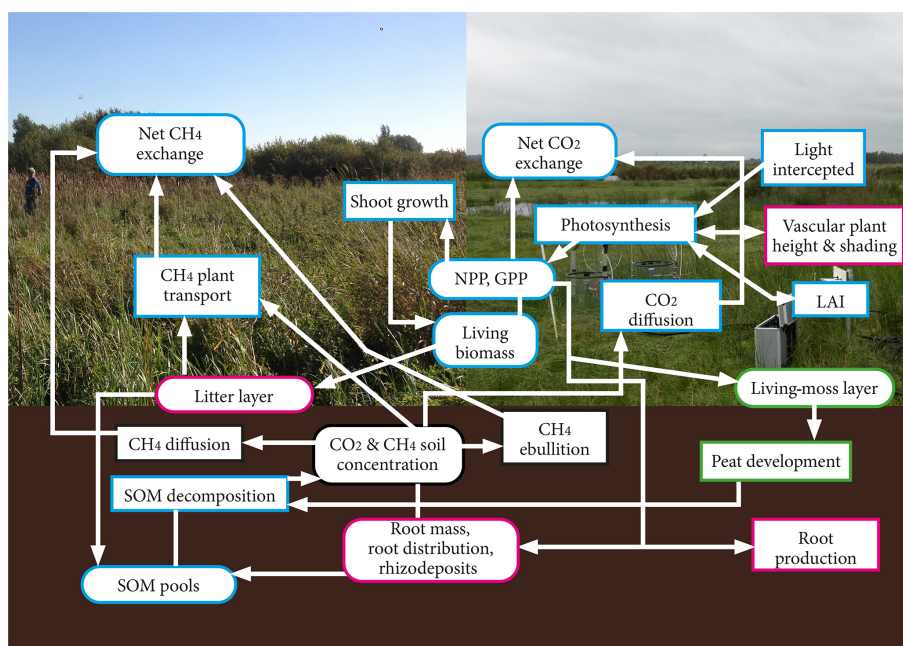
Figure 1. Schematic of the movement of carbon in the model. Processes are delineated with rectangles, whereas carbon pools are delineated with curved edges. The pink outline represents non-moss pools and processes, the green outline represents pools and processes applicable only to moss PFTs, and the blue outline refers to pools and processes that are applicable to all plant types. In the background of this figure, the Horstermeer site is shown on the left, and the Ilperveld site is shown on the right.

and peatlands, two peatland-specific PFTs (flood-tolerant C_3 graminoids and *Sphagnum* mosses), a new decomposition scheme when under inundation, and the addition of root exudates. LPJ-WHyMe particularly assesses the impacts of inundation on vegetation composition, net primary production, and the deceleration of decomposition under inundation.

To assess the impact of dynamic vegetation classes on subsequent GHG fluxes in peatlands, we present a new model, Peatland-VU-NUCOM v1.0 (PVN). PVN incorporates features of NUCOM-BOG, a bog ecosystem model (Heijmans and Berendse, 2008), into the Peatland-VU model framework, a process-based peatland model (van Huissteden et al., 2006). The NUCOM-BOG model simulates vegetation competition and C, nutrient, and water cycling in undisturbed bog ecosystems under changing climates using a soil profile divided by an acrotelm–catotelm boundary where plant growth and decomposition are partitioned between plant organs. The Peatland-VU model simulates the CH_4 and CO_2 cycle within a column of peat soil with varying water levels. The Peatland-VU model simulates CH_4 fluxes, gross primary productivity, and CO_2 cycle whilst assuming a constant plant layer, and it does not include a nitrogen cycle. We have developed a model that, with the appropriate site input data, can be used to simulate peatland sites with a wide variety of vegetation types and vegetation management practices. For this reason, there is no limit to the number of PFTs that can be included in a model simulation. The inclusion of dynamic vegetation classes into the PVN model provides a model that is capable

of estimating the greenhouse gas balance in response to environmental changes (changes in temperature, radiation, precipitation or evapotranspiration, or water levels) and also different management efforts (changes in harvest regime or vegetation restoration) for peatland sites. The incorporation of features of NUCOM-BOG, a model simulating undisturbed systems, into PVN, a new model simulating disturbed and managed systems, requires that changing environmental conditions and changing management practices both lead to dynamic impacts on vegetation classes. Therefore, this model can serve wetland management by estimating changes in the greenhouse gas balance of peatland sites in response to management decisions whilst considering the effects of environmental change.

2 Materials and methods

2.1 The PVN model

The new PVN model describes the vegetation, CH_4, and CO_2 dynamics of a column of an above- and belowground peatland ecosystem (Fig. 1). Carbon dioxide and CH_4 emissions enter the atmosphere by ebullition, transport through plants, diffusion through the soil, and respiration. The aboveground carbon pools are the aboveground living biomass, litter layer (non-moss PFTs only), shoots, and living-moss depth (moss PFTs only). The belowground carbon pools are the peat, la-

bile organic matter, microbial biomass, litter and dead roots, and root exudates (Table S2).

Plant functional types (PFT) are the key element of NU-COM that is added to the Peatland-VU framework to create the PVN model. Any number of PFTs can be included in a model simulation. PFT attributes (parameters) describe plant physiology and bioclimatic limits. Bioclimatic limits are used by the photosynthesis function (Sect. 2.1.1) and the potential growth function (Eq. 13). Each PFT is defined as being either a moss or vascular plant type, which impacts the ability of plants to grow vertically or to develop roots. Each PFT is prescribed as having either evergreen or deciduous phenology. For deciduous vegetation, leaf senescence increases when the daily temperature falls below the PFT's minimum tolerated temperature, whereas, for evergreen vegetation, leaf senescence refers to the death of old leaves (Eq. 9). Maximum leaf coverage is maintained as long as the daily water level and temperature are within the ideal range. The PFT parameters are defined in Table 1, and the references are listed in Table S3. In this section, the subscript p is used to show that the equation or variable is PFT specific, z is used to indicate that the equation or variable is soil layer specific, t is used to represent time, T represents temperature, and WL represents water level. The convention used in this paper is such that a positive flux represents the movement of gas from the ecosystem to the atmosphere.

2.1.1　Primary production

C3 photosynthesis, leaf respiration (RT), and net primary production (NPP) are calculated using a modified version of the primary production scheme introduced into the Peatland-VU model by Mi et al. (2014), modified from the BIOME3 equilibrium biosphere model Haxeltine and Prentice (1996). The BIOME3 model is based on the premise that GPP and leaf respiration increase with the activity of (Rubisco) photosynthetic enzymes in leaf chloroplasts. Photosynthesis is calculated using stomatal conductance and Rubisco activity of leaves. The net CO_2 fluxes (NEE) for each PFT are the sum of gross primary production (GPP [$kg\,C\,m^{-2}\,d^{-1}$]) minus plant respiration, CO_2 produced by belowground aerobic SOM decomposition, and CO_2 oxidised from CH_4 (Rox).

$$GPP_{t,p} = \frac{JE_{t,p} + JC_{t,p} - \sqrt{\dfrac{(JE_{t,p} + JC_{t,p})^2}{-4 \cdot JE_{t,p} \cdot JC_{t,p}}}}{20 \cdot WSF_{t,p}} \quad (1)$$

In the above equation, JE [$kg\,C\,m^{-2}\,d^{-1}$] describes the relationship of photosynthesis to photosynthetically active radiation (PAR), and JC [$kg\,C\,m^{-2}\,d^{-1}$] describes the Rubisco-limited rate of photosynthesis. JE and JC are defined by Eqs. (S2) and (S10) in the Supplement, respectively (Haxeltine and Prentice, 1996; Mi et al., 2014). Interactions among leaf area development, photosynthetic activity, stomatal conductance, temperature, and water availability have

been widely recognised (Baldocchi and Harley, 1995; Koebsch et al., 2020). Water stress has a significant impact on plant photosynthetic capacity (Keenan et al., 2010). Studies such as those of Ostle et al. (2009) and Puma et al. (2013) have considered these factors when simulating GPP by introducing water use efficiency terms. Model intercomparison efforts have found improved reproducibility of GPP estimates from models that account for the impacts of water stress on photosynthetic capacity (De La Motte et al., 2020; Churkina et al., 1999). GPP in the PVN model is modified by both a water stress factor (WSF [–], Eq. S1) and a temperature stress factor (ϕ_T, Eq. S4, adapted from Mi et al. (2014)).

$$NPP_{t,p} = GPP_{t,p} - \int_z^0 Rd_{t,p}\,dz - RT_{t,p} \quad (2)$$

In the above equation, NPP represents the net primary productivity [$kg\,C\,m^{-2}\,d^{-1}$], RT [$kg\,C\,m^{-2}\,d^{-1}$] represents daily leaf respiration, and Rd [$kg\,C\,m^{-3}\,d^{-1}$] represents the root respiration (Eq. 16). Total daily root respiration is the sum of root growth, which varies with depth and is dependent on the root distribution (17).

$$RT_{t,p} = Rr_p \cdot VM_{t,p} \quad (3)$$

In the above equation, Rr [–] is the leaf respiration coefficient (Table 1), and VM [$kg\,C\,m^{-2}\,d^{-1}$] represents the maximum daily rate of net photosynthesis (Eq. S11, Haxeltine and Prentice (1996); Mi et al. (2014)). The CO_2 flux from each soil layer (B_{CO_2}) is calculated before integrating over all layers; it is then summed with CO_2 produced by decomposed litter (LLd [$kg\,C\,m^{-2}\,d^{-1}$]), and NPP is subtracted.

$$NEE_{t,p} = \int_z^0 B_{CO_2,t,p,z}\,dz + LLd_{t,p} - NPP_{t,p} \quad (4)$$

In the above equation, NEE [$kg\,C\,m^{-2}\,d^{-1}$] is the net ecosystem exchange, and B_{CO_2} [$kg\,C\,m^{-3}\,d^{-1}$] is the CO_2 flux produced by belowground SOM decomposition (Eq. 27).

2.1.2　Competition among PFTs

Biomass fraction (BF) is a representation of the ratio of PFT biomass to total biomass (Eq. 5). The sum of all PFTs is constrained to a maximum BF of 1.0. All PFTs have a minimum BF of 0.1 and are able to further establish when the conditions become favourable, as adapted from the NUCOM-BOG model (Heijmans and Berendse, 2008).

$$BF_{t,p} = \frac{CB_{t,p}}{\sum_{p=1}^P (CB_{t,p})} \quad (5)$$

In the above equation, CB [$kg\,C\,m^{-2}$] represents aboveground living biomass (Eq. 9). Each plant competes for light

Table 1. Name, units, description, and values of PFT input parameters. Associated references are listed in Table S3. In the left column, each PFT parameter is tied to its relevant model mechanism. Note that some PFT parameters are, at times, used by multiple model processes.

Corresponding model process	Parameter	Units	Description	Tall grass	Sedges	Typha	Sphagnum	Brown moss	Short grass
Aboveground biomass	BS	–	Fraction of aboveground biomass converted to litter	0.04	0.04	0.04	0.01	0.015	0.03
	KL	–	Fraction of biomass converted to litter during autumn for deciduous plants	0.1	0.1	0.1	0.01	0.04	0.06
	CBiomassRatio	–	Carbon-to-biomass ratio	0.46	0.46	0.46	0.44	0.44	0.44
	RS	–	Fraction of growth that consists of shoots, remainder is root growth	0.7	0.7	0.7	1.0	1.0	0.9
	MaxCanopyHeight	m	Maximum height	1.5813	2.5813	2.5813	0.1	0.2	0.4
Photosynthesis & respiration	$T_{MaxPhoto}$	°C	Maximum temperature for photosynthesis	38	40	35	30	30	30
	$T_{MinPhoto}$	°C	Minimum temperature for photosynthesis	−3	−1	−3	−1	0.5	−1
	T_{min}	°C	Minimum temperature for growth	7	2	2	−1	0.5	0.5
	T_{minopt}	°C	Lowest temperature for optimal growth	9	12	12	14	5	14
	T_{maxopt}	°C	Highest temperature for optimal growth	20	30	30	25	25	25
	T_{max}	°C	Maximum temperature for growth	45	45	45	38	38	38
	Rc	–	Leaf maintenance respiration coefficient	0.015	0.015	0.015	0.016	0.014	0.014
	Rr	–	Leaf respiration coefficient	0.015	0.015	0.015	0.016	0.014	0.014
	Gmax	$g\,C\,d^{-1}$	Maximum growth rate	0.07	0.07	0.07	0.045	0.05	0.05
LAI	SLA	$m^2\,g^{-1}$	Ratio of leaf area to dry leaf mass	0.012	0.012	0.012	0.02	0.02	0.02
	MinLAI	$m^2\,m^{-2}$	Minimum LAI	0.1	0.1	0.1	0.1	0.1	0.1
	MaxLAI	$m^2\,m^{-2}$	Maximum LAI	3	4	4	1.2	1.5	1.5
	LEC	–	Light extinction coefficient	0.5	0.46	0.5	0.95	0.95	0.95
CH$_4$ scheme	PlOx	–	Fraction of CH$_4$ consumed by rhizospheric oxidation	0.4	0.4	0.25	0.7	0.8	0.6
	vP	–	Vegetation type factor for gas transport through plants	5	6	10	2	2	2
Root processes	MRD	m	Maximum root depth	0.46	1	1	0.1	0.1	0.2
	RSX	d^{-1}	Proportion of root mass that dies during each time step	0.05	0.05	0.05	0.01	0.01	0.05
	REX	–	Fraction of belowground production that consists of exudates	0.1	0.2	0.2	0.0	0.0	0.11
	KSP	–	Coefficient for stronger exudation in spring	0.2	0.4	0.4	0.0	0.0	0.1
Belowground decomposition	LC	d^{-1}	Conversion factor of aboveground to belowground litter. 0 °C, LC is set to 0.	0.005	0.001	0.001	0.01	0.005	0.003
	HU	–	Fraction of decomposed organic material transferred to resistant humus fraction	0.55	0.42	0.3	0.9	0.9	0.9
	MI	–	The amount of carbon from decomposed organic matter converted to microbial biomass	2.25	2.2	2.2	2.4	2.3	2.3

Table 1. Continued.

Corresponding model process	Parameter	Units	Description	Tall grass	Sedges	*Typha*	*Sphagnum*	Brown moss	Short grass
Water level	WL_{min}	m	Minimum water level for growth	−1	−1	−1	−0.5	−0.35	−0.35
	$\text{WL}_{\text{minopt}}$	m	Lowest water level for optimal growth	−0.4	−0.3	−0.4	−0.2	−0.15	−0.15
	$\text{WL}_{\text{maxopt}}$	m	Highest water level for optimal growth	−0.2	−0.2	0	−0.05	−0.05	−0.05
	WL_{max}	m	Maximum water level for growth	0.0192	0.1	0.3	0.05	0.05	0.05

where taller PFTs have a monopoly over shorter PFTs. Light that is not intercepted by the tallest PFT becomes available to the next PFT in descending height order. Light that is not intercepted by the vascular PFTs ($_{\text{v}}$) is passed on and divided between moss PFTs ($_{\text{mp}}$) proportionally to their BF. In this way, an increase in the foliage of taller PFTs may reduce the growth rates of mosses due to shading by limiting light exposure. At each time step, vascular PFTs are ordered according to descending height so that the shading by taller PFTs impacts the amount of light available to shorter PFTs. The height of vascular PFTs is calculated using an allometric relationship (Eq. 6) adapted from Huang et al. (1992); Smith et al. (2001); Krinner et al. (2005), which relates vegetation biomass to height. This relationship, initially intended to be used for trees, has since been used to calculate the heights of natural and agricultural grasses in a dynamic global vegetation model (Krinner et al., 2005). Biomass and stem density have been found to respectively explain 98 % and 81 % of the height variance in 65 plots of 29 different species (Gorham, 1979) because most plants are understood to be constrained by self-thinning under crowding in natural stands or by a trade-off between height and foliage growth, reflecting a trade-off between structural and functional physiological development.

$$H_{t,v} = k_2 \cdot \left(\frac{4 \cdot \text{CB}_{t,v}}{\text{BD} \cdot \pi \cdot k_2} \right)^{\frac{k_3}{2+k_3}} \tag{6}$$

In the above equation, H refers to plant height [m]; BD represents biomass density [kg C m^{-3}], k_2 [m]; and k_3 [–] are constants with values of 40 and 0.85, taken from Smith et al. (2001). FPAR [–] is the fraction of incoming PAR absorbed by vegetation (Eq. 7) and is dependent on LAI and the amount of shading by taller plants.

$$\text{FPAR}_{t,p} = 1 - e^{(-\text{LEC}_p \cdot \text{LAI}_{t,p})} \tag{7}$$

In the above equation, LEC represents the light extinction coefficient parameter [–]. LAI [$\text{m}^2 \text{m}^{-2}$] is calculated as a function of living biomass and the specific leaf area (SLA

[$\text{m}^2 \text{kg}^{-1}$ C]).

$$\text{LAI}_{t,p} = \begin{cases} \text{MinLAI}_p, & \text{if } \text{LAI}_{t,p} < \text{MinLAI}_p \\ \text{CB}_{t,p} \cdot \text{SLA}_p, & \text{if } \text{MinLAI}_p \leq \text{LAI}_{t,p} \\ & \leq \text{MaxLAI}_p \\ \text{MaxLAI}_p, & \text{if } \text{LAI}_{t,p} > \text{MaxLAI}_p \end{cases} \tag{8}$$

In the above equation, CB [kg C m^{-2}] represents aboveground living biomass (Eq. 9), dependent on shoot growth and biomass senescence lost to the litter layer.

$$\frac{\delta}{\delta t} \text{CB}_{t,p} = \text{SM}_{t,p} - \text{BS}_{t,p} \cdot \text{CB}_{t,p} \tag{9}$$

In the above equation, SM represents shoot mass [$\text{kg C m}^{-2} \text{d}^{-1}$], calculated using Eq. (10), and $\text{BS}_{t,p}$ represents the fraction of aboveground biomass littered each day [d^{-1}]. Biomass senescence, BS_p [d^{-1}], is set to KL_p [d^{-1}] during autumn for deciduous plants.

$$\text{SM}_{t,p} = \text{RS}_p \cdot \text{NPP}_{t,p} \tag{10}$$

In the above equation, RS [–] represents the ratio of shoot to root growth (Table 1). The allocation of root and shoot growth is a fixed fraction of NPP so that the fraction of shoot and root growth sums to 1.0. The growth of moss PFTs (HG, Eq. 11) is represented in terms of fractional cover rather than height. A moss PFT with more cover has access to more light and gains an advantage over other mosses. Moss PFTs develop at different rates due to differences in the range of temperatures and water levels needed for growth. The depths (or thickness [m]) of both individual moss PFTs (Eq. 11) and the total living-moss layer (Eq. 12) are dependent on BF, potential growth, and dry bulk density (DBD [kg C m^{-3}]). The thickness of the living-moss layer is not yet used by the model. Future model versions will use the thickness of the moss layer to recalculate land surface height, impacting the water level relative to the surface and also the soil properties (such as the DBD, pH, and OM content of top soil layer(s)).

$$\text{HG}_{t,\text{mp}} = \frac{\text{PG}_{t,\text{mp}} \cdot \text{BF}_{t,\text{mp}}}{\text{DBD}_{t,\text{mp},z=1}} \tag{11}$$

In the above equation, $_{mp}$ represents moss PFTs only, and PG represents potential growth (PG [–], Eq. 13). The moss thicknesses of individual moss PFTs are aggregated to calculate the total ecosystem moss depth (MHG [m]):

$$\text{MHG} = \frac{\sum_{\text{mp}=1}^{\text{MP}} (\text{HG}_{t,\text{mp}} \cdot \text{BF}_{t,\text{mp}})}{\sum_{\text{mp}=1}^{\text{MP}} \text{BF}_{t,\text{mp}}}. \tag{12}$$

Potential growth (PG [–], Eq. 13) reflects the favourability of water levels or temperatures for PFT growth, calculated using the water growth (WG [–]) and temperature growth (TG [–]) functions, respectively. Potential growth, WG, and TG are adapted functions from Heijmans and Berendse (2008).

$$\text{PG}_{t,p} = \text{FPAR}_{t,p} \cdot \text{Gmax}_p \cdot \text{TG}_{t,p} \cdot \text{WG}_{t,p} \tag{13}$$

In the above equation, Gmax is the maximum growth rate [$\text{kg C m}^{-2}\,\text{d}^{-1}$]. The WG and TG functions are congruent with each other, where unfavourable temperature or water levels reduce growth.

$$\text{WG}_{t,p} = \begin{cases} 0, & \text{if } \text{WL}_t < \text{WL}_{\text{min},p} \\ \frac{\text{WL}_t - \text{WL}_{\text{min},p}}{\text{WL}_{\text{minopt},p} - \text{WL}_{\text{min},p}}, & \text{if } \text{WL}_{\text{min},p} \leq \text{WL}_t \\ & \quad < \text{WL}_{\text{minopt},p} \\ 1, & \text{if } \text{WL}_{\text{minopt},p} \leq \text{WL}_t \\ & \quad \leq \text{WL}_{\text{maxopt},p} \\ \frac{\text{WL}_{\text{max},p} - \text{WL}_t}{\text{WL}_{\text{max},p} - \text{WL}_{\text{maxopt},p}}, & \text{if } \text{WL}_{\text{maxopt},p} < \text{WL}_t \\ & \quad \leq \text{WL}_{\text{max},p} \\ 0, & \text{if } \text{WL}_t > \text{WL}_{\text{max},p} \end{cases} \tag{14}$$

In the above equation, WL refers to water level, min and max refer to the minimum and maximum water levels tolerated for growth, and minopt and maxopt refer to the minimum and maximum optimum water levels for growth.

$$\text{TG}_{t,p} = \begin{cases} 0, & \text{if } T_t < T_{\text{min},p} \\ \frac{T_t - T_{\text{min},p}}{T_{\text{minopt},p} - T_{\text{min},p}}, & \text{if } T_{\text{min},p} \leq T_t < T_{\text{minopt},p} \\ 1, & \text{if } T_{\text{minopt},p} \leq T_t \leq T_{\text{maxopt},p} \\ \frac{T_{\text{max},p} - T_t}{T_{\text{max},p} - T_{\text{maxopt},p}}, & \text{if } T_t \leq T_{\text{max},p} \\ 0, & \text{if } T_t > T_{\text{max},p} \end{cases} \tag{15}$$

In the above equation, T refers to daily temperature, min and max refer to the minimum and maximum tolerated temperatures for growth, and minopt and maxopt refer to minimum and maximum optimum temperatures for growth.

2.1.3 Belowground production

The root distribution and the root mass of vascular PFTs are mapped to the layout of the model's soil horizon representation (depth, density, and layer thickness). To account for differences in decomposition rates among roots and exudates,

each PFT has designated SOM pools, which are partitioned between the soil layers. Root distribution and root mass decrease exponentially from the surface to the PFT maximum root depth (MRD in Table 1). In general, 30 %, 50 %, and 75 % of roots are observed in the top 10, 20, and 40 cm, respectively (Jackson et al., 1996). Root exudation plays an important role in the rhizosphere by promoting methanogenesis and soil carbon loss through CH_4 production. The production of new roots (Rd) is based on a PFT-prescribed shoot-to-root-growth ratio and NPP. Root exudates (RX, Eq. 19) are a fraction of the calculated belowground root production (Rd). Exudates develop at a prescribed rate per PFT, dependent on root and shoot growth. Photosynthesis rates are enhanced during spring and summer and are accompanied by the highest levels of root and soil respiration (Högberg et al., 2001). There is strong evidence to suggest that enhanced photosynthesis fuels exudate production, causing seasonal variation in exudation (Whipps, 1990; Saarnio et al., 2004). The root growth and die-off functions are adapted from van Huissteden et al. (2006).

$$\text{Rd}_{t,v,z} = (1 - \text{RS}_v) \cdot \text{NPP}_{t,v} \cdot f(z, p) \tag{16}$$

In the above equation, $1 - \text{RS}$ represents the fraction of growth that is root growth, and $f(z, p)$ [m^{-1}] represents the exponential root distribution from the surface to the maximum root depth (MRD in Table 1).

$$\int_{-\text{MRD}_p}^{0} f(z, p)\,\text{d}z = 1 \tag{17}$$

$$\frac{\delta}{\delta t} \text{RM}_{t,v,z} = \text{Rd}_{t,v,z} - \text{RX}_{t,v,z} - \text{RDR}_{t,v,z} \tag{18}$$

In the above equation, RM is the root mass [kg C m^{-3}]. RDR [$\text{kg C m}^{-3}\,\text{d}^{-1}$] represents the death of existing roots.

$$\text{RX}_{t,v,z} = \text{Rd}_{t,v,z} \cdot f(\text{KSP}_{v,\text{DoY}}) \cdot \text{REX}_{t,v} \tag{19}$$

In the above equation, DoY represents the day of the year; REX [–] represents the unitless root exudation factor; and $f(\text{KSP})$ [–] is a function depending on the PFT constant, KSP (Table 1), that can be used to determine when stronger exudation occurs during spring.

$$\text{RDR}_{t,v,z} = \text{RM}_{t,v,z} \cdot \text{RSX}_v \tag{20}$$

In the above equation, RSX represents the root senescence rate [d^{-1}].

2.1.4 Litter layer production and decomposition

Vegetation composition change directly impacts litter input, which alters the quality and quantity of fresh SOM contributions (Malmer et al., 2005). Senescence of the aboveground living biomass is added to the litter layer for vascular PFTs

(Eq. 21). Senescence of moss PFTs contributes directly to the belowground SOM pools. Movement of surface litter to SOM pools is an important component of peatlands (Davidson and Janssens, 2006). Carbon dioxide produced from the decomposition of the litter layer and the different SOM pools are summed with NEE (Eq. 4).

$$\frac{\delta}{\delta t}LL_{t,v} = LLp_{t,v} - LLl_{t,v} - LLd_{t,v} \tag{21}$$

In the above equation,

$$LLp_{t,v} = BS_v \cdot CB_{t,v}, \tag{22}$$

$$LLl_{t,v} = \frac{T_t}{KT} \cdot LC_p \cdot LL_{t,v}, \tag{23}$$

$$LLd_{t,v} = LL_{t,v} \cdot e^{ke_L}, \tag{24}$$

where LLp [kg C m^{-2} d^{-1}] refers to litter production, and LLl [kg C m^{-2} d^{-1}] refers to litter lost to belowground SOM. Biomass senescence (BS$_p$ [d^{-1}]) is set to KL$_p$ [d^{-1}] during autumn for deciduous plants (Table 1), LC [d^{-1}] is the fraction of litter converted to SOM each day, KT [°C] is the reference temperature, and T [°C] represents the daily air temperature. Litter does not decompose if the daily temperature falls below zero. ke$_L$ [kg C m^{-2} d^{-1}] refers to the rate of litter decomposition, adjusted by an environmental correction factor (Eq. S18, van Huissteden et al. (2006)).

2.1.5 Belowground SOM decomposition

Peatlands consists of organic compounds at different stages of decomposition. In the model, these belowground organic components are separated into five SOM pools (peat, humus, microbial biomass, litter and dead roots, root exudates) (Table S2). Each of the SOM pools lose and gain mass, whilst the number and the thicknesses of the soil layers remain constant throughout the model simulation. Biodegradation of SOM leads to the mineralisation of carbon that can be reincorporated into SOM and repeatedly recycled (Basile-Doelsch et al., 2020). This means that some SOM pools are active (microbial biomass, litter and dead roots, root exudates), whilst others are passive (humus, peat). Active carbon pools are available for microbial decomposition and then partitioned between CO$_2$ and CH$_4$, where passive carbon pools decompose very slowly. Vascular plants generally have faster decomposition rates than mosses (Graf and Rochefort, 2009); therefore, vascular plants contribute to only one of the two passive SOM pools (humus, Table S2), whereas moss PFTs contribute to both passive SOM pools (humus and peat). The decomposition of each SOM pool is calculated assuming first-order rate kinetics:

$$\frac{\delta}{\delta t}Q_{t,p,z,s} = -ke_{t,s} \cdot Q_{t,p,z,s}, \tag{25}$$

where SOM pools are represented by the subscript s, Q [kg C m^{-3}] represents the mass of organic carbon in each

SOM pool, and ke [d^{-1}] represents the decomposition rate for each SOM pool adjusted by an environmental correction factor (Eq. S18, van Huissteden et al. (2006)).

$$SD_{t,p,z} = \sum_{s=1}^{S}(ke_{t,s} \cdot Q_{t,p,z,s}) \tag{26}$$

In the above equation, SD [kg C m^{-3} d^{-1}] represents the total carbon lost from all SOM pools. A fraction of the decomposed carbon from the SOM pools (litter and dead roots, root exudates, peat) is transferred (mineralised and reincorporated) into microbial biomass and humus, and the remaining fraction of SD is transferred into CO$_2$. The CO$_2$ flux from the decomposition of SOM is calculated per soil layer:

$$B_{CO_2,t,p,z} = SD_{t,p,z} \cdot (1 - FMI_{p,z} - HU_{p,z}) + Rox_{t,p,z} \cdot MC, \tag{27}$$

$$FMI_{p,z} = \frac{1 - HU_{p,z}}{1 + MI_{p,z}}, \tag{28}$$

where FMI [–] refers to the fraction of SOM transferred to the microbial biomass pool, calculated using the PFT parameter MI [–] (Table 1); HU [–] refers to the fraction of SOM transferred to the resistant humus pool; Rox [μM CH$_4$ m^{-3} d^{-1}] represents the portion of CH$_4$ oxidised to CO$_2$ (Eq. S27); and MC [kg C μM CH$_4^{-1}$] represents the conversion factor (from μM CH$_4$ to kg C).

2.1.6 Methane processes

The daily CH$_4$ flux is dependent on the production and oxidation of CH$_4$, as well as on the three transport mechanisms (diffusion, ebullition, and plant-transported CH$_4$). The CH$_4$ flux at the soil surface (Eq. 29) is calculated by summing the three transport mechanisms (diffusion, ebullition, and plant-transported CH$_4$). The CH$_4$ concentration of each soil layer (Eq. S19) is calculated before summing all transport mechanisms at the soil surface to obtain the net flux. Methane processes were adapted from the Peatland-VU model (van Huissteden et al., 2006), originally described in Walter and Heimann (2000).

$$Ft_{t,p} = \sum_{p=1}^{P}(Fpl_{t,p}) + Fdiff_{t,z=0} + Feb_t \tag{29}$$

In the above equation, Ft [μM m^{-2} d^{-1}] represents the total daily CH$_4$ flux at the soil surface; Fpl [μM m^{-2} d^{-1}] represents the total plant-transported CH$_4$ flux (Eq. 31); Fdiff [μM m^{-2} d^{-1}] is the diffusive flux at the soil/water–atmosphere boundary, $z = 0$ (Eq. S20); and Feb [μM m^{-2} d^{-1}] is the ebullitive flux (Eq. S24). Methane production (Eq. S26), oxidation (Eq. S27), ebullition (Eq. S25), and diffusion of CH$_4$ through the soil (Eq. S20) remain as described in van Huissteden et al. (2006), originally adapted from Walter and Heimann (2000).

Plant-transported CH_4 is calculated for each PFT. There are two mechanisms which determine the amount of CH_4 lost via plant transport. Firstly, the mass and distribution of the root system play a role in determining how much CH_4 is taken up into the plant tissue. Thereby, a dense or large root system enables more CH_4 to enter the plant tissue. When CH_4 passes through the oxic zone around the root tips, a fraction of CH_4 is consumed by rhizospheric oxidation (Schipper and Reddy, 1996). This is represented by the unitless PFT parameter, PlOx (Eq. 31). Secondly, the amount of CH_4 transported through the plant tissue and released to the atmosphere is determined by its aerenchyma. Plants with large aerenchyma are efficient transporters of CH_4. The PFT parameter vP [–] describes the plant's ability to conduct CH_4 through aboveground plant tissue (Table 1). Shrubs and trees generally do not have aerenchyma, whereas grasses and sedges can have large or small aerenchyma (Ström et al., 2005; Walter and Heimann, 2000). The values for these PFT parameters are taken from the literature and are cited in Table S3.

$$Qpl_{t,p,z} = -cP \cdot vP_p \cdot LAI_{t,p} \cdot f(z,p) \cdot C_{CH_4,t,z} \qquad (30)$$

In the above equation, Qpl [$\mu M\,m^{-3}\,d^{-1}$] represents the plant-transported CH_4, cP [$m^{-2}\,day^{-1}$] is a rate constant with a value of 0.24 (taken from Walter and Heimann (2000)), $f(z,p)$ [m^{-1}] represents the exponential root distribution (Eq. 17), and C_{CH_4} [$\mu M\,m^{-3}$] represents the CH_4 concentration. The rate of plant-transported CH_4 is integrated over the depth of the root zone to obtain the flux at the surface (Eq. 31):

$$Fpl_{t,p} = \int_{MRD}^{0} \left[Qpl_{t,p,z} \cdot (1 - PlOx_p) \right] dz, \qquad (31)$$

where Fpl represents the total plant-transported CH_4 flux [$\mu M\,m^{-2}\,d^{-1}$].

2.1.7 Harvest scheme

If the harvest scheme is activated in the model input file, PFTs taller than the prescribed harvest height are harvested (mowed) at the prescribed date. This is a relevant feature for agricultural (e.g. Knox et al. (2015)) or other managed peatlands (e.g. Evans et al. (2021)). The harvest height and days are, therefore, optional prescribed model parameters. Living biomass decreases according to the amount of biomass harvested because biomass is assumed to be uniformly distributed with height and is not partitioned into organs. LAI is recalculated (Eq. 8), and the PFT height is set to the harvested height. A fixed fraction of the harvested material is assumed to be lost during the harvest process, remains uncollected in the field, and is added to the litter layer. This fraction can also be set to zero.

2.2 Two peatland sites

With this study, the PVN model simulates two peatland sites in the Netherlands, the Horstermeer site and the Ilperveld site (Fig. S1). The Ilperveld site (52°26′° N, 4°56′° E; 1.42 m below sea level (m b.s.l.)) is currently a nature recreation area that is a former raised bog complex that was drained to be used as agricultural pasture and is frequently exposed to manure fertilisation (van Geel et al., 1983; Harpenslager et al., 2015). Since the early 2000s, the Ilperveld site has undergone restoration efforts which included raising the water level, removal of the fertilised and nutrient-rich top soil, attempts to re-introduce *Sphagnum*, and water quality management. The vegetation consists of brown mosses, *Sphagnum*, and grasses (*Poaceae* family). Since restoration began, the site has been mown twice a year, in June and September. Vegetation profiles show layers of intact *Sphagnum* and *Carex* peat, and, unlike undisturbed peatlands, the top layer has undergone greater decomposition due to land management since drainage (Harpenslager et al., 2015). The Horstermeer site (52°15′° N, 5°04′° E; 2.1 m b.s.l.) lies on the Horstermeer polder and is a former drained agricultural peat meadow that has not been used since the 1990s, when the water level was also raised. It was used for grazing and was exposed to manure fertilisation until the 1990s. The Horstermeer site is now a semi-natural fen containing very heterogeneous vegetation, including reeds, grasses, and small shrubs, and is not subject to mowing or other land management practices (Hendriks et al., 2007). Vegetation consists of different types of grasses and sedges (the dominant species are *Holcus lanatus*, *Phalaris arundinacea*, and *Glyceria fluitans*) and reeds (*Phragmites australis* and *Typha latifolia*). The Horstermeer polder is subject to strong seepage of mineral-rich groundwater from surrounding lake areas and Pleistocene ice-pushed ridges (Hendriks et al., 2007). The Horstermeer polder was a freshwater lake that was drained as part of large-scale land reclamation project completed in 1888.

2.3 PFT attributes

This study defined six PFTs (*Typha*, sedges, tall grasses, short grasses, *Sphagnum*, brown mosses) based on the vegetation communities observed at the Horstermeer and Ilperveld sites. PFT attributes (Table 1) were amalgamated from the NUCOM-BOG model, the TRY 5.0 database (https://www.try-db.org, last access: 18 May 2022) (Kattge et al., 2011, 2020), and other relevant publications listed in Table S3. As much as possible, PFT parameter values are informed by observational data (Kattge et al., 2011, 2020; Heijmans et al., 2008). Sedges, tall grasses, and *Typha* all represent graminoids with deep root systems that can grow at a range of water levels but have different aerenchyma and growing ranges. Sedges are from the families *Cyperaceae* and *Juncaceae* and are grass-like, monocotyledonous flowering plants with aerenchymae. Tall grasses are from the fam-

ily *Poaceae* and are grass-like plants with elongated, long, blade-like leaves without aerenchyma. *Typha* PFTs represent a genus of about 30 species of monocotyledonous flowering plants in the family *Typhacea* with large aerenchyma. The short grasses PFT is representative of forbs and agricultural-like grasses with shallow root systems. The *Sphagnum* PFT is representative of hummock *Sphagnum* species which are generally more drought tolerant. Brown mosses represent all non-*Sphagnum* mosses but have similar but slightly broader temperature growth ranges. The SOM evolved from short grasses decomposes more easily than the SOM evolved from brown mosses, which decomposes more easily than the SOM evolved from *Sphagnum*. The six PFT input parameter sets used in this study are accessible from the Bitbucket repository: https://www.bitbucket.org/tlippmann/pvn_public (last access: 15 November 2023).

2.4 Model calibration

The model was calibrated to reproduce fluxes that fall within the spread of observed in situ chamber measurements measured at the Horstermeer and Ilperveld peatland sites (Sect. 2.2). The PVN model simulates processes at a daily time step. We ran the model using 28 years (1990–2017, inclusive) of input data (Sect. 2.7) for the Horstermeer and Ilperveld sites. The length of the model spin-up was 5 years, determined by the time taken for the SOM pools, belowground CO_2, and belowground CH_4 concentrations to stabilise (Fig. S4). Thereby, the first 5 years of model simulations (1990–1995) are considered as the spin-up period. Daily CO_2 and CH_4 fluxes measured at the Horstermeer and Ilperveld sites between 2015 and 2017 were used to calibrate the model. Unfortunately, there were not enough data to split the observational data into separate datasets for calibration and validation.

A Monte Carlo analysis was performed separately for each site to calibrate 13 model parameters (Table S4). Parameters without available observational data were included in the model calibration process. The Kling–Gupta efficiency (KGE) metric was used to measure the agreement between simulated and observed CO_2 and CH_4 fluxes (Gupta et al., 2009; Kling et al., 2012). The KGE approach is a three-dimensional decomposition of the Nash–Sutcliffe efficiency (NSE) measure and evaluates temporal dynamics, bias, and variability Eq. (28). The KGE metric has been used to assess the ability of carbon flux models (Tramontana et al., 2016; Zhao et al., 2020), hydrological models (Dick et al., 2015), and meteorological reanalysis datasets (Chaney et al., 2014; Muñoz-Sabater et al., 2021) to reproduce in situ observations. The calibrated model input values are provided in Tables S6 and S7 for the Horstermeer and Ilperveld site simulations, respectively.

The CO_2 results impact the CH_4 results much more than the CH_4 results impact the CO_2 results; therefore, we first ensured that the parameters impacting the photosynthesis and the above- and belowground growth and respiration schemes reproduced fluxes that fell within the spread of observed CO_2 fluxes (NEE). These were the MolAct, HalfSatPoint, and VegTScalingFactor parameters. Next, the CH_4 scheme was calibrated to reproduce fluxes that fell within the spread of observed CH_4 fluxes. This involved calibrating the remainder of the parameters highlighted in Table S4. Even though the amount of photosynthesis and living biomass does not directly impact the CH_4 production, which primarily occurs in the soil and aboveground litter layers, these processes are precursors to root and shoot growth, respiration, and senescence, which directly impact simulated CH_4 fluxes. After optimisation of the CH_4 fluxes, the PFT parameters (Table S3) were manually adjusted to bring the PFT biomass fractions (PFT biomass as a fraction of total biomass) in line with observed aerial cover fraction ratios. The calibrated model parameters and the necessary input files used to simulate the two peatland sites evaluated in this study are accessible from the Bitbucket repository: https://www.bitbucket.org/tlippmann/pvn_public (last access: 15 November 2023).

2.5 Testing the PVN model

To understand the sensitivity of net CO_2 and CH_4 fluxes to PFT-dependent processes, we conducted several model simulations using modified input data. Air temperature, water table, radiation, harvest, and the swapping of PFTs between site simulations were chosen to be used for the sensitivity testing because they are key environmental drivers of CO_2 and CH_4 emissions in peatlands. We tested the sensitivity of PFT processes by varying these inputs one by one (Table 2).

To understand how the new model mechanisms affect emissions, we performed additional simulations with altered model algorithms and compared these to the original model simulations calibrated for the Horstermeer and Ilperveld sites (Table 3). For example, the contribution of competition for shading to the overall simulation result is quantified by comparing an altered simulation where incoming photosynthetically active radiation (PAR) is independent of shading (e.g. fractional par or FPAR = 0.25 for a simulation with four PFTs) to the original model simulations (FPAR_CONST). We calculated the relative difference of the simulation with shading minus the simulation without shading. Similarly, we compared simulations with and without plant-transported CH_4 (CH4_OLD_CF), with and without dynamic BF (CF_CONST), and with and without variable plant height (HEIGHT_CONST).

In order to demonstrate that the PVN model reproduces CH_4 and CO_2 fluxes within the spread of observed fluxes when driven by realistic input data, we compared the calibrated model simulation results and measured CH_4 and CO_2 fluxes for the Horstermeer and the Ilperveld field sites (Sect. 2.2).

We compare the CH_4 and CO_2 fluxes of the calibrated model simulation results against the CH_4 and CO_2 fluxes

Table 2. A summary of the varied input data used to understand the sensitivity of the model.

Changing input variable	Input change
Air temperature	$\pm 1, \pm 3\,°C$
Harvest frequency	no harvest; once, twice, three, or four times per year
PFTs	Exchange Ilperveld and Horstermeer PFTs*
Radiation	$\pm 8, +100, +200\,J\,m^{-2}$
Water level	$\pm 0.1, \pm 0.2\,m$

* To compare the PFT dynamics, both simulations use the no-harvest regime. The exchange of PFTs means that the model simulation driven by the Ilperveld input data (Table 4) will use the PFTs observed at the Horstermeer site (*Typha*, tall grass, sedges, brown moss), while the model simulation driven by the Horstermeer input data will use the PFTs observed at the Ilperveld site (short grass, tall grass, *Sphagnum*, brown moss).

Table 3. A summary of the simulations with altered model algorithms.

Simulation name	Mechanism change
CH4_OLD_CF	Uses Peatland-VU CH_4 module multiplied by the PFT cover fraction
CF_CONST	Biomass fraction is constant for all PFTs, i.e. BF $= 0.25$
FPAR_CONST	FPAR is constant for all PFTs, i.e. FPAR $= 0.25$
HEIGHT_CONST	Constant plant height for each PFT

simulated by the Peatland-VU model to understand the impact of introducing PFTs on the simulation of CH_4 and CO_2 fluxes. These model simulations are summarised in Table 4. Attempts to run the Peatland-VU model with new calibrated parameters did not yield results on the same order of magnitude as the observations. Therefore, it was necessary to use different model parameterisations for the PVN and Peatland-VU models.

2.6 Flux measurements

Carbon dioxide and CH_4 fluxes were measured using two to four automated flux chambers (AC) and the Ultra-Portable Los Gatos Gas Analyser Model 915-001. Chambers were cylindrical, 30 cm wide and 40 cm in height, made of transparent acrylate, equipped with a fan, and installed in the field using collars. Where necessary, vegetation was folded gently to fit inside the measurement chambers. Collars were removed from the field between sampling campaigns, which minimises disturbance which can lead to potential biases in the observations. This also potentially introduces uncertainty with regard to the precise measurement location. The CO_2 and CH_4 concentrations were measured for 150 s intervals whilst the chamber was closed. Each chamber was measured on rotation so that a new chamber was measured every 15 min. Measurements were recorded continuously during the day and night for a week at a time, during which time the AC system was moved to another site. We note that, due to the labour-intensive nature of accumulating chamber observations consistently through time, these observational datasets do not offer complete temporal continuity, creating an intermittency bias. From these data, the hourly average

CO_2 (net ecosystem exchange) and CH_4 fluxes were calculated for each day. We compared calibrated site simulations against observed daily average CO_2 and CH_4 fluxes. To visualise the daily variability, standard deviations were derived from the hourly fluxes. The values for all GHG emissions are expressed as CO_2 equivalents $[kg\,CO_{2eq}\,m^{-2}\,yr^{-1}]$ and are calculated as

$$GHG_{CO_2 e} = CH_4 \cdot GWP + CO_2, \qquad (32)$$

where $GWP_{20} = 80.8$ as $1\,kg\,CH_4 = 80.8\,kg\,CO_2$ eq. over a 20-year time horizon, and $GWP_{100} = 27.2$ as $1\,kg\,CH_4 = 27.2\,kg\,CO_2$ eq. over a 100-year time horizon (Masson-Delmotte et al., 2021).

2.7 Input data preparation

The PVN model is driven by daily air temperature (T), water level (WL), radiation, a general model parameter input file (Table S4), and a soil parameter input file (Table S5).

2.7.1 Climatological input data

Daily temperature and radiation data, measured at Schiphol, the nearest KNMI weather station, were used as climate input data for both sites (accessed via https://www.knmi.nl/nederland-nu/klimatologie/daggegevens, last access: 18 May 2022) (Fig. S3). The annual average rainfall at Schiphol was $850\,mm\,yr^{-1}$ over the period 1990–2020, with 30 % of the rainfall falling in summer and autumn and 24 % falling in winter, with the remainder falling in the spring. The average daily temperature between 1990 and 2019 was 9.4 °C and warmed by approximately $+0.1\,°C\,yr^{-1}$

over the same period. The average daily temperature for the warmest month, August, was 22.1 °C, and the lowest daily monthly temperature for the coldest month, January, was 0.8 °C.

2.7.2   Soil profile input data

The model generates a soil horizon representation using soil layers of 10 cm thickness. The generated soil horizon uses properties such as the dry bulk density (DBD), SOM ratio, sand content, and C:N ratio specified in the soil profile input data (Table S5). The number and depths of the site's soil horizons can be adjusted in the soil input file. The PVN model requires input parameters for each PFT, as discussed in Sect. 2.3. Soil profile data from the Horstermeer and Ilperveld field sites were collected in 2015 and 2016 and include DBD, C content, SOM content, sand and clay content, and pF curve (Tables S8 and S9 for the Horstermeer and Ilperveld site simulations, respectively).

2.7.3   Water level input data

Water level input data were sourced from the Dutch hydrological model, the Netherlands Hydrological Instrument (NHI) (De Lange et al., 2014), which has a reasonably high spatial resolution (250 m × 250 m). One aim of developing the PVN model is to eventually develop a model of all Dutch peatlands in conjunction with the NHI product. For this reason, the NHI product is used in this application of the model. The NHI water level output was converted to relative surface height using a 5 m × 5 m digital elevation map of the Netherlands, Actueel Hoogtebestand Nederland (Alhoz et al., 2020). It is possible to use in situ water levels as input data for the model, but these data were, unfortunately, unavailable for the duration of the simulation. The input data used for both sites are accessible from the Bitbucket repository: http://www.bitbucket.org/tlippmann/pvn_public (last access: 15 November 2023).

3   Results

When describing the annual CO_2, CH_4, and GHG values, we opt to use the term emissions, e.g. annual GHG emissions, whereas, when describing daily values, we opt to refer to these as fluxes, e.g. daily GHG fluxes.

3.1   Model sensitivity to input data

To understand the response of the modelled PFT processes to input data, we ran simulations with modified water levels (Figs. 3 and S6), temperature (Figs. 2 and S5), and radiation (Fig. S7) input and harvest schemes (Fig. 4). The modified input data are summarised in Table 2, and the results of these sensitivity tests are summarised in Table 5. These results are indicative of the model's mechanistic responses

rather than being projections of how PFTs might respond under varied environmental conditions. To show how different inputs impact model processes, we present the soil (respiration) CO_2 emissions (Fig. 3), plant-transported CH_4 (Fig. 2), and aboveground biomass (Fig. 4). In the PVN model, the abundance of each PFT varies through time depending on the favourability of growing conditions. Therefore, an increase in CO_2 or CH_4 emissions may be due to increased abundance (i.e. enhanced biomass) or enhanced transport efficiency. To disentangle this difference, the CO_2 and CH_4 emissions for each PFT are plotted as a fraction of litter and root mass.

Increased air temperatures had a positive effect on both plant-transported CH_4 emissions (Fig. 2) and litter and root mass at both sites (Fig. S5). Short and tall grasses showed similar responses to increased air temperatures by producing large CH_4 emissions per kilogram of litter and root mass. Brown mosses showed little variation between the temperature experiments for the Ilperveld site but showed a decrease in emissions with warming temperatures per kilogram of litter and root mass at the Horstermeer site. *Sphagnum* similarly showed a decrease in CH_4 emissions with warming temperatures per kilogram of litter and root mass at the Ilperveld site. This decrease is because moss PFTs have strict ideal-temperature growth limits (T_{max} and T_{min} in Table 1) and were limited by warming temperatures. Whilst belowground, CH_4 concentrations increased with warming temperatures, and the biomass, litter, and root mass of moss PFTs did not increase with warming temperatures.

Belowground CO_2 emissions were impacted by changing water levels (Fig. S6). Previous studies have found that belowground CO_2 production tends to increase with low water levels due to enhanced potential for aerobic CO_2 production (Knox et al., 2015). The results of the Ilperveld site sensitivity simulations showed that belowground CO_2 production increased with low water levels, likely due to enhanced potential for aerobic CO_2 production. However, the results of the Horstermeer site sensitivity simulations showed the converse: that the net CO_2 (Table 5) and belowground CO_2 production increased with high water levels. We simulate that, with high water levels, the reduced aerobic CO_2 production can be exceeded by the enhanced oxidation of CH_4 into CO_2. The large amounts of CH_4 oxidised into CO_2 in the Horstermeer site simulation are due to the very degraded peat present at the site (represented by low soil OM content in the soil input file) and the strong upwelling of rich groundwater at the Horstermeer site (represented by the calibratable model parameter, MolAct (see Sect. 2.4), which influences the sensitivity of aerobic CO_2 production). The large observed CH_4 emissions at the Horstermeer site are partially due to high CH_4 concentrations in the upwelling water. Furthermore, the large root systems of plants such as *Typha*, sedges, and tall grasses have greater potential to access and transport stores of belowground gases (represented by the PFT root depth and mass). The conflicting response of the tall grass PFT in the

Table 4. A summary of the model simulations using both the new PVN model and the pre-existing Peatland-VU (PV) model. Model input parameters for the Horstermeer and Ilperveld site simulations are provided in Tables S6 and S7, respectively.

Site	Model	Vegetation	Harvest height
Horstermeer	PVN	*Typha*, sedges, tall grass, brown moss	–
Horstermeer	PV	–	–
Ilperveld	PVN	Short grass, tall grass, brown moss, *Sphagnum*	0.15 m
Ilperveld	PV	–	0.15 m

Table 5. The results of the sensitivity testing. The CH_4 and CO_2 columns indicate how much the respective emissions changed when the input changed relative to the results of the respective default Horstermeer and Ilperveld PVN simulations described in Table 4. A dash [–] indicates that the simulation is the default site simulation. An overview of the sensitivity tests can be found in Table 2.

Changing input variable	Input change	Horstermeer		Ilperveld	
		CH_4 [%]	CO_2 [%]	CH_4 [%]	CO_2 [%]
Air temperature	$+3\,°C$	165	117	115	122
	$+1\,°C$	128	94	102	108
	$-1\,°C$	77	93	100	87
	$-3\,°C$	56	66	154	53
Harvest frequency	no harvest	–	–	120	129
	$1\,yr^{-1}$	114	68	87	117
	$2\,yr^{-1}$	114	67	–	–
	$3\,yr^{-1}$	115	67	152	70
	$4\,yr^{-1}$	114	68	185	45
PFTs	*Typha*, sedges, tall grass, brown moss	–	–	291	294
	Short grass, tall grass, brown moss, *Sphagnum*	35	68	–	–
Radiation	$+200\,J\,m^{-2}$	121	107	97	126
	$+100\,J\,m^{-2}$	111	104	98	113
	$+8\,J\,m^{-2}$	101	101	98	101
	$-8\,J\,m^{-2}$	99	99	98	99
Water level	$+0.2\,m$	149	104	200	99
	$+0.1\,m$	134	103	172	100
	$-0.1\,m$	98	98	87	101
	$-0.2\,m$	163	97	281	101

Ilperveld and Horstermeer simulations shows that PFTs may respond differently to changing water levels at different sites.

Increasing the frequency of harvests led to a strong negative effect on vascular plant biomass and a small positive effect on moss plant biomass (Fig. 4). The biomass of non-moss PFTs is strongly impacted by the occurrence of harvests, as indicated by the pause in biomass accumulation after harvest. However, by reducing tall vegetation, moss species have greater access to sunlight and, therefore, gain an advantage. For this reason, we saw the biomass of moss PFTs increase with more frequent harvests. In the Horstermeer site simulation, the greatest effect on biomass was between no harvests and the once-per-year harvests. In the Ilperveld site simulation, the effects of harvests on biomass increased somewhat linearly according to the frequency of harvest events. We suspect that this is due to the inclusion of different PFTs in the two site simulations. In the Horstermeer site simulation, three PFTs have the capacity to grow above the harvest height (the *Typha*, tall grass, and sedge PFTs), whereas in the Ilperveld site simulation, only tall and short grasses have the potential to grow beyond the harvest height, thereby limiting the potential effect harvests can have on the PFTs present. Furthermore, the growth of the short grass PFT is height limited to 0.3 m. Overall, total biomass was reduced with more frequent harvest regimes.

It is important to note that, whilst CO_2 emissions were reduced by increasing the frequency of harvests, these emissions do not account for the off-site decomposition of harvested biomass. Methane emissions were slightly enhanced if harvests occurred in comparison to no harvest events for Horstermeer site simulations, whilst the frequency of harvests did not impact emissions (Table 5). Similarly, enhanced
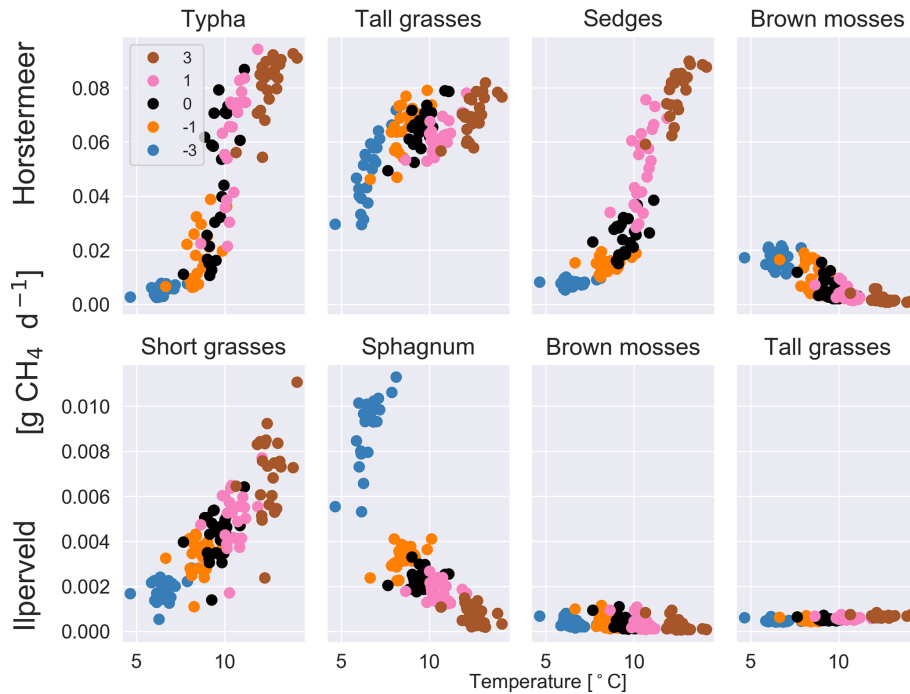
Figure 2. The results of the sensitivity tests show the relationship between different temperature inputs and the mean daily plant-transported CH_4 for each year for each of the PFTs at the Horstermeer site (top row) and Ilperveld site (bottom row). Temperature input was increased and decreased by 1 and 3 °C, respectively. The legend shows the input change [°C] where ± signs in front of the legend labels show the direction of change. Note the different y axes between the top and bottom panels.

Figure 3. The results of the sensitivity tests show the relationship between different water level inputs and the mean daily soil CO_2 flux for each year for each of the PFTs at the Horstermeer site (top row) and the Ilperveld site (bottom row). Water level input was decreased by 0.1 and 0.2 m and was increased by 0.1 and 0.2 m, respectively. The legend shows the input change, where ± signs in front of the legend labels indicate the direction of the change. Note the different y axes between the top and bottom panels.

CH_4 emissions occurred with increased harvest frequency for the Ilperveld site simulations. Spikes in CH_4 fluxes transported by vascular PFTs occurred after harvest events in both the Horstermeer and Ilperveld simulation results (not shown), contributing to enhanced CH_4 emissions for both the Ilperveld and Horstermeer site simulations. The impact of fewer or no harvest events led to variable impacts on CH_4 emissions for the Ilperveld site simulations, where a single harvest led to slightly reduced emissions, and no harvests led to slightly enhanced emissions. In the Ilperveld site simulation without harvest events, vegetation became dominated by vascular PFTs that are efficient transporters of CH_4, leading to enhanced CH_4 emissions.

3.2   Assessment of model mechanisms

To understand the role of isolated model mechanisms, we modified the model code to disable the functions responsible for reproducing the vegetation dynamics within the model (Fig. 5). Unlike the other simulations assessed throughout this paper, the simulation results shown in Fig. 5 begin in the year 1990, i.e. without the use of a spin-up period. Removing the spin-up period showed that the modified model simulation results produce similar emissions in the first year of the simulation (1990) and allows an assessment of the trajectory of deviation.

Disabling the shading scheme (simulation PVN_HEIGHT_CONST) or biomass fraction scheme (simulation PVN_CF_CONST) led to only slightly enhanced CO_2 emissions, whereas disabling the FPAR scheme (simulation PVN_FPAR_CONST) led to large CO_2 emission differences. Surprisingly, the difference for the PVN_FPAR_CONST simulation is opposite in sign for the two site simulations and is larger for the Ilperveld simulation. This means that maintaining constant FPAR led to a small enhancement in CO_2 emissions in the Horstermeer simulation but a large reduction in CO_2 emissions for the Ilperveld simulation. These results show that FPAR plays a large role in simulated CO_2 emissions. The results of the Ilperveld PVN_FPAR_CONST simulation also showed that the FPAR function has the potential to introduce large variability into the emission results. This is interesting to note because the PVN model showed limited skill in reproducing the CO_2 emissions at the Ilperveld site. These results indicate that the function calculating FPAR plays a driving role in CO_2 emissions but particularly at the Ilperveld site. Further model developments may investigate ways to improve the representation of FPAR in the model. The PVN_FPAR_CONST simulations also led to enhanced CH_4 emissions for the Ilperveld simulation. It is likely that CH_4 production was enhanced due to increased stores of CO_2.

The use of the Peatland-VU CH_4 scheme (PVN_CH4_OLD_CF) led to large differences in CH_4 emissions for both the Horstermeer and Ilperveld simula-

tions in comparison to the PVN model results. The CH_4 emissions of the model simulations that use the Peatland-VU CH_4 scheme (simulation PVN_CH4_OLD_CF) were small when compared to the CH_4 emissions of the PVN model for both model simulations. This indicates that the PFT modifications to the CH_4 scheme have led to substantial impacts on modelled CH_4 emissions.

3.3   Assessment of calibrated model simulations

Here, we describe the simulation results of the model calibrated at two field sites, Horstermeer and Ilperveld. We describe the net annual CH_4 and CO_2 emissions and GHG budgets (Fig. 6), as well as the simulated PFT dynamics as indicated by changes to LAI, aboveground biomass, litter mass, and PFT height and/or depth (Figs. 7 and S8). All net GHG values are expressed as CO_2 equivalents (CO_2 eq.). The model simulation results indicate that the simulated annual mean net GHG emissions from the Ilperveld simulation were approximately half the emissions of the Horstermeer simulation. However, these model emission estimates do not consider off-site decomposition of harvested biomass. The model estimated that the 2015–2017 annual average net GHG emissions were 2.5 and $8.9 \, kg \, CO_2 \, eq. \, m^{-2} \, yr^{-1}$ for the Ilperveld and Horstermeer simulations, respectively (Table 6), calculated using the 20-year GWP. Using the 100-year GWP, the 2015–2017 annual average net GHG emissions were 2.3 and $5.6 \, kg \, CO_2 \, eq. \, m^{-2} \, yr^{-1}$ for the Ilperveld and Horstermeer simulations, respectively. The model estimated that the 1995–2017 annual average net GHG emissions were 2.4 and $8.0 \, kg \, CO_2 \, eq. \, m^{-2} \, yr^{-1}$ for the Ilperveld and Horstermeer model simulation results, respectively (Fig. 6), calculated using the 20-year GWP. Using the 100-year GWP, the 1995–2017 annual average net GHG emissions were estimated to be 2.3 and $5.2 \, kg \, CO_2 \, eq. \, m^{-2} \, yr^{-1}$ for the Ilperveld and Horstermeer model simulation results, respectively.

Assessment of the Horstermeer simulation showed that, on average, CH_4 contributed approximately half (52 %) of the net annual GHG emissions of the Horstermeer simulation, where CH_4 contributed $4.2 \, kg \, CO_2 \, eq. \, m^{-2} \, yr^{-1}$ and CO_2 emissions contributed $3.8 \, kg \, CO_2 \, eq. \, m^{-2} \, yr^{-1}$, on average. Assessment of the Ilperveld simulation showed that CO_2 was the primary contributor to net GHG emissions, where CO_2 contributed the majority (92 %) of the annual GHG emissions ($2.2 \, kg \, CO_2 \, eq. \, m^{-2} \, yr^{-1}$ of the total $2.4 \, kg \, CO_2 \, eq. \, m^{-2} \, yr^{-1}$ net GHG emissions). These model emission estimates neglect the off-site decomposition of harvested biomass. Therefore, CO_2 and CH_4 emissions contribute equally to the net GHG emissions in the Horstermeer simulation, whereas CO_2 emissions dominate the GHG emissions in the Ilperveld simulation results.

To assess whether there was an increasing or decreasing trend in emissions over the duration of the simulation (1995–2017), we calculated the linear regression of the CO_2,
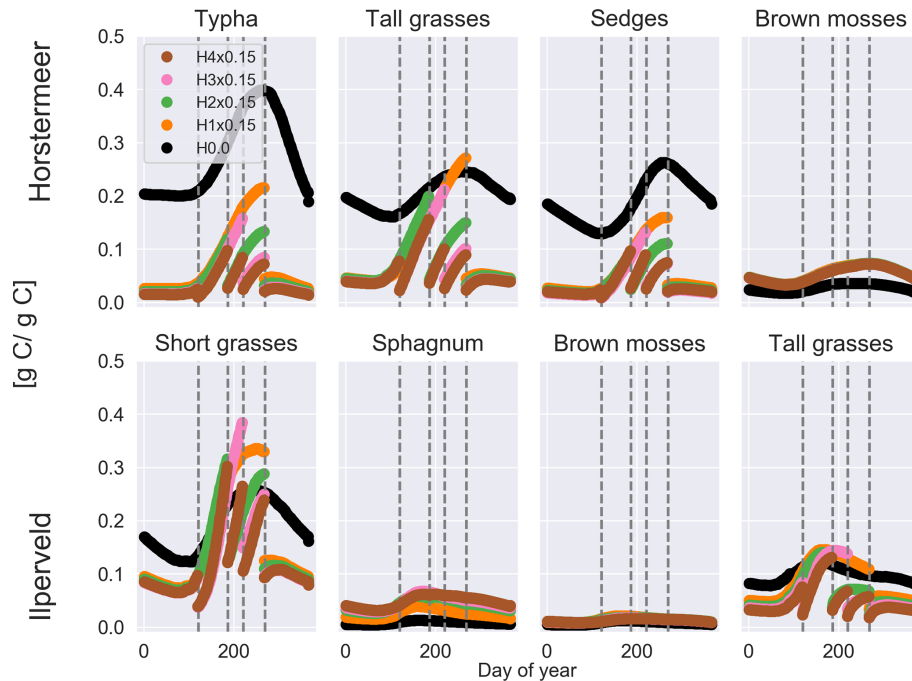
Figure 4. The results of the sensitivity tests show the relationship between different harvest schemes and biomass for each day of year (shown as a fraction of litter and root mass) at the Horstermeer site (top row) and Ilperveld site (bottom row). Vegetation is cut to 0.15 m (×0.15) at the moment of harvest. The legend shows the harvest input scheme, and the vertical dotted lines indicate the four possible harvest days (days 120, 186, 220, and 268). Harvest was set to either not occur (H0.0) or to occur once per year (H1x0.15) on day 268, twice per year (H2x0.15) on days 186 and 268, three times per year (H3x0.15) on days 120, 220 and 268, or four times per year (H4x0.15) on all harvest days.
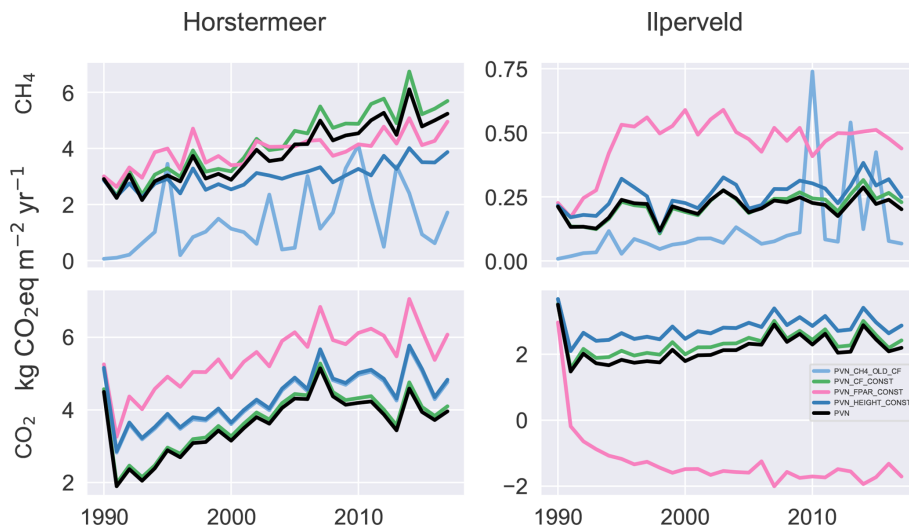
Figure 5. The CH_4 and CO_2 emissions for various isolated model mechanisms compared against the PVN model result. We investigated maintaining constant fractional PAR (PVN_FPAR_CONST), maintaining constant plant height (PVN_HEIGHT_CONST), maintaining constant cover fraction (PVN_CF_CONST), and including the original Peatland-VU CH_4 module multiplied by the PFT cover fraction (PVN_CH4_OLD_CF) at each time step.

CH_4, and net GHG time series of the simulation results at both sites. The trends of the Horstermeer simulation emission results were 0.13, 0.06, and 0.19 kg CO_2 eq. m^{-2} yr^{-1} for CH_4, CO_2, and the net GHG emissions. Daily temper-

ature observations show that local temperatures increased by +0.1 °C yr^{-1} between 2010 and 2017 or +0.06 °C yr^{-1} over the entire simulation period (1995–2017). The trend results for the Ilperveld simulation emissions were zero for
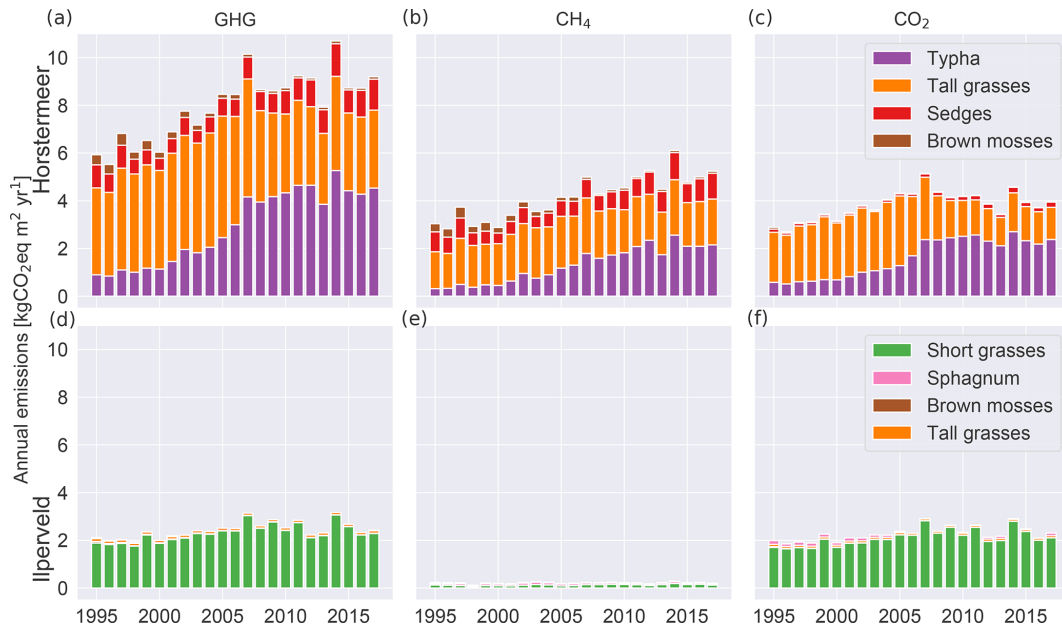
Figure 6. Relative contributions of each PFT to simulated annual average net GHG (**a, d**), CH$_4$ (**b, e**), and CO$_2$ (**c, f**) emissions. The results of the Horstermeer site simulation are represented in (**a**)–(**c**), and the results of the Ilperveld site simulation are represented in (**d**)–(**f**).

CH$_4$ emissions and $0.04 \, \mathrm{kg\,CO_2 \, eq. \, m^{-2} \, yr^{-1}}$ for CO$_2$ and net GHG emissions. Warming temperatures are a possible driver of the enhanced GHG emissions at the Horstermeer site. The increase in GHG emissions in the Horstermeer site simulation and the little or no increase in the Ilperveld site simulation are aligned with the results of the $+1\,°\mathrm{C}$ temperature sensitivity tests. The results of the Horstermeer site sensitivity tests showed that the *Typha* and sedge PFTs were sensitive to warming temperatures; therefore, the increases in the biomass and GHG emissions of the *Typha* and sedge PFTs at the Horstermeer site are likely due to enhanced temperatures.

3.3.1 PFT dynamics

Here, we describe the living biomass, LAI, litter layer, biomass fraction, and height changes of the PFTs of the calibrated Horstermeer and Ilperveld model simulations (Figs. 7 and S8). Assessment of the aboveground biomass (top row of Fig. 7) shows that the tall grass (blue line), *Typha*, and sedge PFTs (red line) were abundant during the Horstermeer simulation, whereas the Ilperveld simulation was dominated by the short grass (green line), *Sphagnum* (pink line), and tall grass PFT (blue line). All plants showed seasonal variability. The ratio of the litter layer to biomass is between approximately 1 : 4 and 1 : 3 for most PFTs [kg C]. The *Typha* PFT is an exception, and the ratio is approximately 1 : 1. Overall, the sedge PFT showed comparable seasonal variability to the tall grass PFT whilst maintaining less biomass, smaller LAI, and shorter height throughout the Horstermeer simulation. The similar behaviour of the *Typha*, sedge, and tall grass PFTs was expected because the PFT input parameters represent similar plant phenologies. Assessment of the size of the litter layer (first row of Fig. S8) showed that, in the Ilperveld simulation, the PFTs reached peak litter during autumn (September), whilst in the Horstermeer simulation, which is not mown, the litter continued to accumulate until January, where rates of decomposition exceeded accumulation. The LAI (second row of Fig. S8) displayed strong seasonal variability. Each year, the LAI of the short grasses reaches its maximum LAI value of 1.2. The tall grass PFT, whilst very competitive in the Horstermeer simulation, is less competitive in the Ilperveld simulation, partially due to the occurrence of harvests and partially because it is outcompeted by the fast-growing short grass PFT. Assessment of the Ilperveld simulation reveals that the short grass PFTs were constrained by the maximum-height parameter, MaxCanopyHeight. The tall grass PFT was not limited by MaxCanopyHeight in the Ilperveld simulation but was instead limited by the biannual mowing regime. PFT height showed strong seasonal variability for both simulations (third row of Fig. S8). The tall grass PFT constituted the tallest plants in the Horstermeer simulation until 2009, and its height was frequently limited by the PFT MaxCanopyHeight parameter. However, as the *Typha* PFT grew in biomass, the tall grass PFT appeared to have less access to sunlight as height and biomass values were reduced. The *Typha* and sedge PFTs were not limited by their maximum-height parameters. These changes in biomass fraction are also evident in the emissions.

The relative contributions of each PFT to the net annual CH$_4$, CO$_2$, and GHG emissions are shown in Fig. 6, where the CH$_4$ emissions refer to only the plant-transported CH$_4$. The net CO$_2$ emissions for each PFT are the sum of the
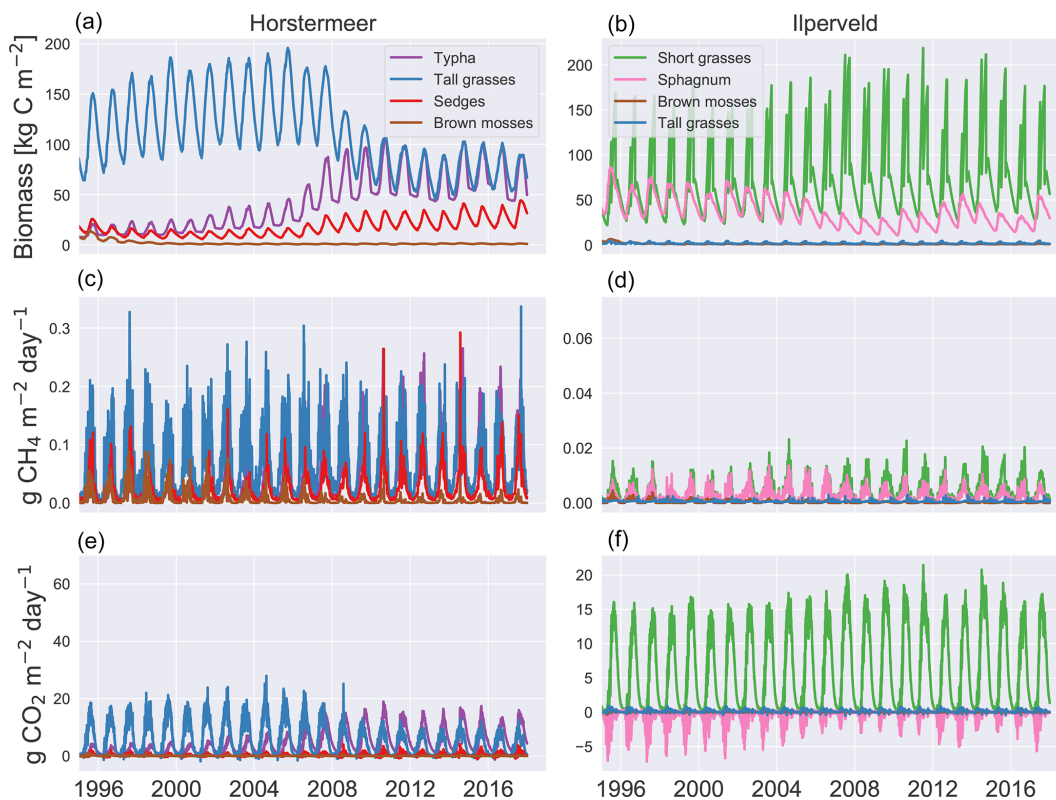
Figure 7. Vegetation dynamics. The results of the Horstermeer site simulation are represented in **(a)**, **(c)**, and **(e)**, and the results of the Ilperveld site simulation are represented in **(b)**, **(d)**, and **(f)**. Note the differing y axes.

photosynthesis minus respiration, the CO_2 produced by belowground aerobic decomposition of SOM, and a portion of CH_4 oxidised to CO_2. The tall grass (red boxes), sedge (orange boxes), and *Typha* (purple boxes) PFTs are large transporters of CH_4 emissions in the Horstermeer simulation results. However, only the tall grasses and *Typha* compose the net CO_2 emissions in the Horstermeer simulation. Thereby, the tall grass PFT was the largest contributor to the net annual GHG emissions, followed by the *Typha* and sedge PFTs. The Ilperveld simulation results showed that the short grass PFT was the largest contributor to the net annual CH_4, CO_2, and GHG emissions.

3.4 Comparison of modelled and observed plant dynamics

We compare simulated PFT biomass fractions against observed aerial plant cover fractions (Fig. 8). For assessment against observational data, we compare model simulation results against observed fluxes by comparing time series, boxplots, and 1 : 1 scatterplots for CH_4 (Fig. 9) and CO_2 (Fig. 10). Gaps in observational data exist due to measurement collection limitations; therefore, the model comparison against observational data can only be shown for the days where observational data exist. Unfortunately, this means that the model was not assessed equally across all seasons

or on the same days of the year at the two sites. A simple linear regression is used to compare the model simulation results and observational data using all days with available measurements. For these reasons, the 1 : 1 plots and R^2 linear regression results may only give a flavour of model performance. To understand the degree of uncertainty in the observational measurements, daily standard deviations were derived using the hourly fluxes (plotted as black error bars in Figs. 9 and 10). In each case, the model simulation results generally lay within the spread of observational uncertainty. The observations indicated that both sites are annual sources of CH_4 and CO_2 and, therefore, net annual sources of carbon to the atmosphere. The Horstermeer site produced large annual mean CH_4 and CO_2 emissions in comparison to the Ilperveld site (Fig. 9 and Fig. 10).

3.4.1 Evaluation of plant composition dynamics

Plant cover fraction observations were made at the location of the chamber measurements and were not representative of the site's complete plant community composition. Although aerial cover fraction and biomass fraction (the ratio of PFT biomass to total biomass) are not the same, changes in plant composition are depicted in both representations.

In 2006, the chamber measurement location at the Horstermeer field site was composed of tall grasses (50 %), sedges
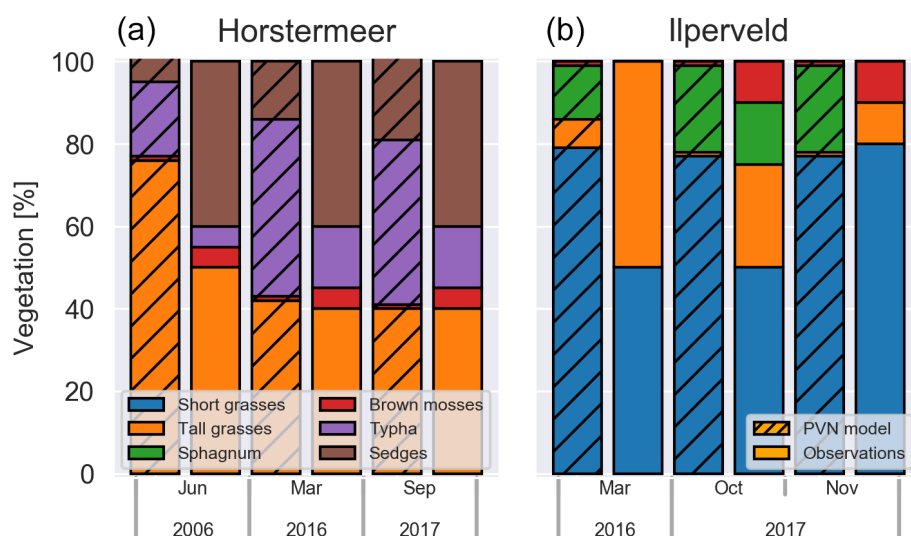
Figure 8. Simulated PFT biomass fractions and observed areal cover fractions at Horstermeer **(a)** and Ilperveld **(b)**.

(40 %), *Typha* (5 %), and brown mosses (5 %) (left panel in Fig. 8). The Horstermeer simulation results show good agreement with the observations but overestimated the amount of tall grasses (66 %) and underestimated the amount of sedges (40 %). In 2016, a decade later, the amount of tall grasses remained consistent, whilst the amount of *Typha* had increased by 10 %; 1 year later, in 2017, the vegetation had not undergone changes proportionally. Parallel to the observations, the Horstermeer simulation results estimated that the tall grass PFTs decreased to 60 % from 2005 onwards, whilst the biomass fractions of the *Typha* and sedge PFTs increased. Overall, the Horstermeer simulation overestimated the biomass fraction of the tall grass PFT and underestimated the proportion of the sedge and *Typha* PFTs. Model estimates of year-to-year PFT biomass changes were of the same sign and similar magnitude as in situ observations.

In March 2016, the chamber measurement location at the Ilperveld field site hosted short grasses (50 %) and tall grasses (50 %). The model overestimated the amount of short grasses (80 %), underestimated the amount of tall grasses (5 %), and overestimated the amount of *Sphagnum* (10 %). The *Omhoog met het Veen* (Raising the Peat) project delivered on-site management attempts to initiate *Sphagnum* growth by hand dispersing living fragments of *Sphagnum* spp. from a nearby donor site between 2013 and 2015 (Geurts and Fritz, 2018). For this reason, we expected that the model may not match the development of *Sphagnum* at the Ilperveld site. In October 2017, the vegetation shifted to be composed of short grasses (50 %) and tall grasses (25 %), *Sphagnum* (15 %), and brown mosses (10 %); 1 month later, in November 2017, the *Sphagnum* was no longer visible (0 %), brown mosses remained (10 %), and the site was dominated by short grasses (80 %). The model estimated that the short grass and *Sphagnum* PFTs remained consistent into 2016 and 2017,

whilst the tall grass PFT was reduced, and brown mosses increased slightly. Whilst the model simulations ended in 2017, we saw that, in October 2018, the vegetation remained constant at both sites.

3.4.2 Evaluation of simulated CH₄ fluxes

The time series presented in Fig. 9 shows the behaviour of the Horstermeer simulation CH_4 flux results (purple line), the observed mean daily fluxes (black dots), and the spread of the hourly observed fluxes (black error bars). Whilst the Horstermeer simulation reproduced the seasonal variability of the observed CH_4 fluxes, the boxplots showed that the simulation results (purple box) tended to overestimate the CH_4 fluxes. Overall, the Horstermeer simulation showed a robust pattern of variability when compared with the observations ($R^2 = 0.7$) whilst overestimating the magnitude of observed fluxes. Assessment of the Ilperveld model simulation showed that the model was able to reproduce the observed CH_4 fluxes and followed the pattern of variability when compared with the observations ($R^2 = 0.8$). The summer of 2015 is an exception where the simulated results showed an increase in CH_4 fluxes larger than the observed CH_4 fluxes. Assessment of the boxplots showed that the simulated CH_4 fluxes (green box) are of a similar mean and spread to the observed fluxes (purple box).

3.4.3 Evaluation of simulated CO₂ fluxes

The boxplots showed that the PVN Horstermeer simulation reproduced the median and range of observed daily CO_2 fluxes at the Horstermeer site. The results of the Horstermeer site simulation (purple line) reproduced the 2015, 2016, and 2017 spring CO_2 fluxes. The results of the Horstermeer site simulation captured the 2015 and 2016 autumn fluxes.
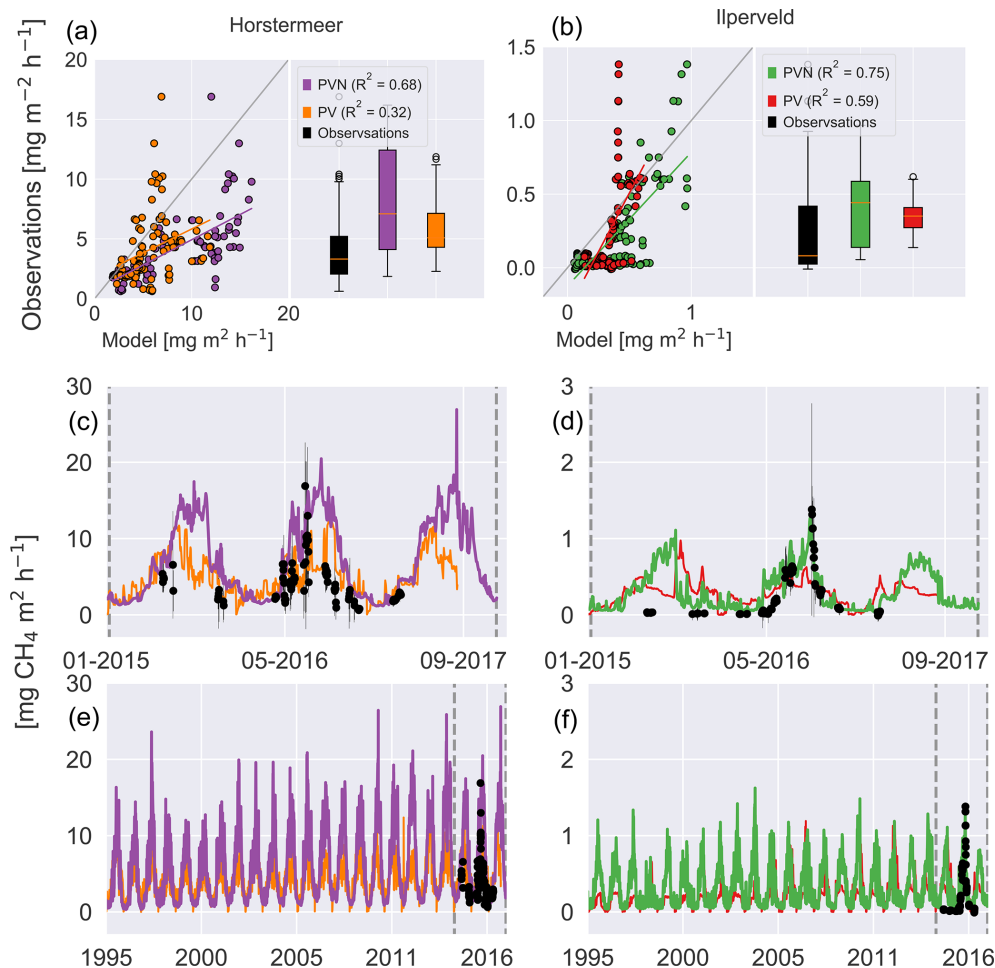
Figure 9. Simulated and observed methane fluxes at the Horstermeer (**a, c, e**) and Ilperveld (**b, d, f**) sites. The R^2 values are provided for comparison between the new PVN, the Peatland-VU model, and the observations. In (**a**) and (**b**), the 1 : 1 line is plotted in grey. The black dots are in situ flux chamber observational measurements in (**c**), (**d**), (**e**), and (**f**). Note the differing x and y axes.

However, the model generally overestimated the magnitude of simulated fluxes (purple box) but generally reproduced the variability ($R^2 = 0.8$).

The boxplots in Fig. 10 showed that the Ilperveld simulation results (green box) generally overestimated CO_2 fluxes. The boxplots showed that the mean hourly CO_2 flux simulated by the model was a small positive flux at $250\,\text{mg}\,CO_2\,\text{m}^{-2}\,\text{h}^{-1}$, whereas the observed mean hourly flux was $0\,\text{mg}\,CO_2\,\text{m}^{-2}\,\text{h}^{-1}$. The Ilperveld simulation (green line) captured the early-spring fluxes in 2016 and 2017. However, during 2015 and 2016, the model tended to overestimate the observed CO_2 fluxes. Comparison of the simulated daily hourly average (green line) and the spread of hourly fluxes (black error bars) showed that the simulated CO_2 fluxes (green line) fell within the spread of daily hourly fluxes. The model showed some agreement with the observed pattern of variability ($R^2 = 0.6$).

The comparison between the Horstermeer simulation results and observations showed that the model captured the

mean daily CO_2 fluxes but overestimated CH_4 fluxes. The comparison between the Ilperveld simulation results and the observations showed that the model overestimated the mean CO_2 fluxes but reproduced the mean and variability of CH_4 fluxes.

3.5 Comparison to the PEATLAND-VU model

To understand the impact of including vegetation dynamics, we compare the results of the new PVN model against the results of the pre-existing Peatland-VU model (Fig. 9 and CO_2 in Fig. 10). The simulation results are summarised in Table 6. Overall, the PVN model estimated the net annual CH_4, CO_2, and GHG emissions to be larger than the emissions estimates made by the Peatland-VU model. The Peatland-VU model estimated the annual mean 2015–2017 GHG emissions to be 1.3 and 5.9 kg CO_2 eq. m^{-2} yr^{-1} for the Ilperveld and Horstermeer simulations, respectively, calculated using a 20-year GWP. When calculated using a 100-year GWP,

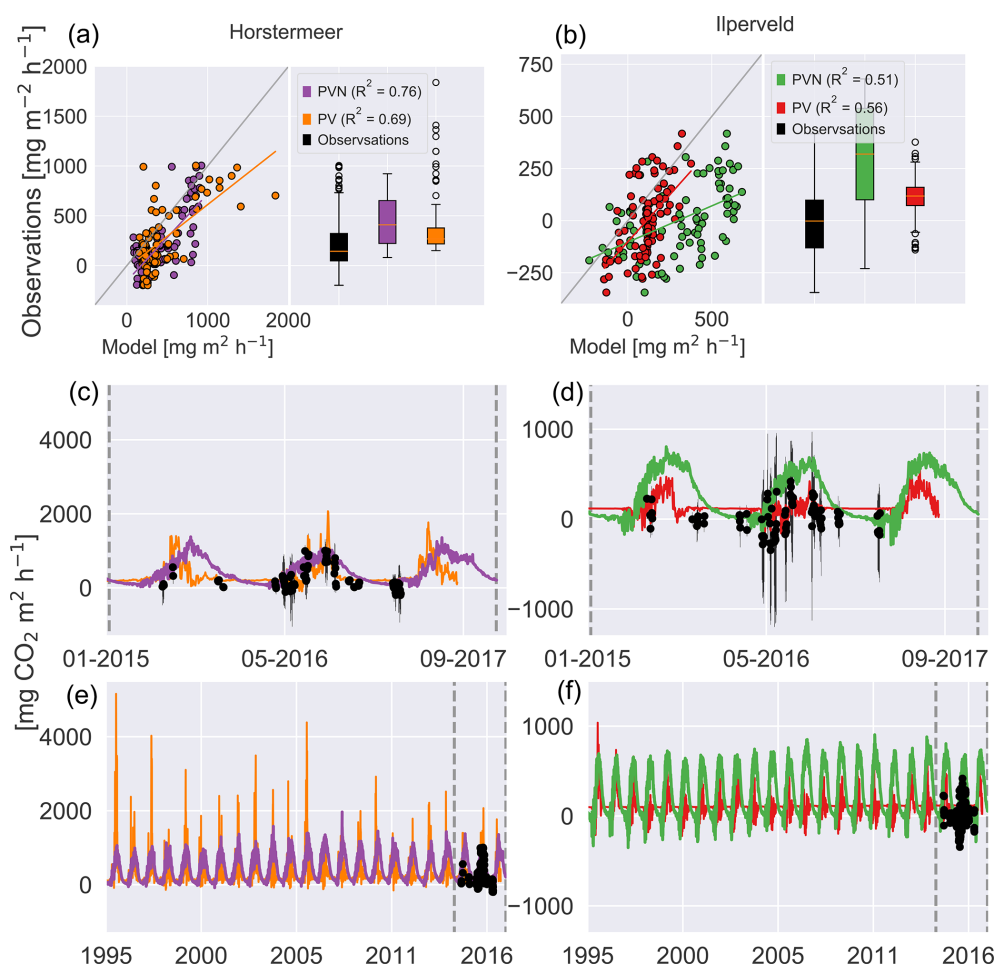**Figure 10.** Simulated and observed carbon dioxide fluxes (NEE) at the Horstermeer **(a, c, e)** and Ilperveld **(b, d, f)** sites. The R^2 values are provided for comparison between the new PVN, the Peatland-VU model, and the observations. In **(a)** and **(b)**, the 1 : 1 line is plotted in grey. The black dots are in situ flux chamber observational measurements in **(c)**, **(d)**, **(e)**, and **(f)**. Note the differing x and y axes.

the Peatland-VU model GHG emission estimates for the Horstermeer simulation were $3.8\,\mathrm{kg\,CO_2\,eq.\,m^{-2}\,yr^{-1}}$ (for both periods of 2015–2017 and 1995–2017). The Peatland-VU GHG emission estimates for the Ilperveld simulation were 1.3 and $1.2\,\mathrm{kg\,CO_2\,eq.\,m^{-2}\,yr^{-1}}$ for the 2015–2017 and 1995–2017 periods, respectively.

The comparison of modelled and measured CH_4 emissions showed that the PVN model performed well, reproducing CH_4 emissions within the spread of observations, in comparison to the Peatland-VU model. The PVN Horstermeer simulation results estimated large mean annual CH_4 emissions $(5.1\,\mathrm{kg\,CO_2\,eq.\,m^{-2}\,yr^{-1}})$ in comparison to the Peatland-VU model $(3.2\,\mathrm{kg\,CO_2\,eq.\,m^{-2}\,yr^{-1}})$ for the period 2015–2017. The R^2 value of the PVN model results in comparison to the observations was 0.7 for the Horstermeer simulation and 0.8 for the Ilperveld simulation. In comparison, the Peatland-VU model results produced R^2 values of 0.3 and 0.6 for the Horstermeer and Ilperveld simulations, respectively. The Peatland-VU model showed good skill in reproducing the

CO_2 fluxes at the Horstermeer site $(R^2 = 0.7)$ and less skill at the Ilperveld site $(R^2 = 0.6)$. Similarly, the PVN model showed good skill in reproducing daily CO_2 fluxes at the Horstermeer site $(R^2 = 0.8)$ but less skill at the Ilperveld site $(R^2 = 0.6)$, as indicated by the linear regression results. Overall, assessment of the linear regression results showed that the behaviour of the PVN model performed well against the observations when compared to the Peatland-VU model.

4 Discussion

We have developed the PVN model, a new dynamic vegetation–peatland–emissions model capable of understanding the role dynamic PFTs play in CO_2 and CH_4 emissions in peatlands. We tested the sensitivity of simulated PFT processes to changing environmental parameters and investigated the impacts of the new schemes introduced into the model that attempt to replicate competition between vegetation types. Here, we discuss potential sources of uncertainty,

Table 6. Annual average 2015–2017 and 1995–2017 CO_2, CH_4, and GHG emissions. All values are expressed as CO_2 equivalents [$kg\,CO_2\,eq.\,m^{-2}\,yr^{-1}$] and are calculated using 20- or 100-year GWP for CH_4 and GHG values.

Site	Model	GHG		CO_2		CH_4	
		2015–2017	1995–2017	2015–2017	1995–2017	2015–2017	1995–2017
Horstermeer	PVN	8.88 (5.56)	7.96 (5.20)	3.87	3.81	5.01 (1.68)	4.15 (1.40)
Horstermeer	PV	5.90 (3.80)	5.80 (3.81)	2.74	2.81	3.17 (1.07)	2.99 (1.01)
Ilperveld	PVN	2.47 (2.32)	2.41 (2.27)	2.25	2.19	0.22 (0.08)	0.22 (0.08)
Ilperveld	PV	1.27 (1.15)	1.19 (1.08)	1.09	1.03	0.18 (0.06)	0.16 (0.05)

both in the observational data used to evaluate the model results and in the chosen model input parameters. Secondly, we discuss the processes in the model that allow the representation of dynamic vegetation and the ability of these processes to respond to changing environments. Lastly, we discuss how the new PVN model compares to its two parent models, the NUCOM-BOG model and the Peatland-VU model, as well as the one other site-specific GHG emissions peatland model that uses dynamic PFTs.

4.1 Sources of uncertainty

4.1.1 Input parameters

It is important to note that the Peatland-VU, NUCOM-BOG, and PVN are heavily parameter-dependent models. The Peatland-VU model has been shown to reproduce observed fluxes using widely different parameter sets, which means that the Peatland-VU model has a strong equifinality of parameterisations (van Huissteden et al., 2009) because there are simply not enough data available to constrain all model dynamics. One aim of introducing PFTs into the Peatland-VU model was to develop a model with a greater dependence on observational data (measurable PFT traits) and less dependence on optimised parameters, reducing the equifinality of the model. It is important that improvements to model processes capture the critical processes but as simply as possible to minimise problems that arise due to the equifinality of parameterisations (Beven and Freer, 2001). The introduction of PFTs allowed several Peatland-VU parameters that were previously calibratable to become observation-informed parameters whilst introducing few new parameters; thereby, the net result is a reduction in the breadth of the parameter space.

4.1.2 Site heterogeneity and chamber measurements

We compare the findings of this study against other studies that have assessed observed CH_4 fluxes at the Horstermeer site and discuss uncertainties accompanying the chamber measurement technique. The sites simulated in this study pose challenges because they are degraded peatlands where easily decomposable carbon is likely to have been mineralised (Dorrepaal et al., 2007; Järveoja et al., 2013), peat has been artificially removed for centuries (Erkens et al.,

2016), and nutrients have been added during livestock grazing (Schrier-Uijl et al., 2014). It remains unclear what impacts these events continue to have on present-day CO_2 and CH_4 fluxes. Unfortunately, at the time of publication, there were no published studies investigating the CO_2 or CH_4 fluxes measured at the Ilperveld site. The CH_4 fluxes observations ($0–17\,mg\,CH_4\,m^{-2}\,h^{-1}$) presented in this study compared well to reported chamber CH_4 fluxes measured at the Horstermeer site from 2003 till 2008 (van Huissteden et al., 2009), in the range of $2–15\,mg\,CH_4\,m^{-2}\,h^{-1}$ at an area of the site with a varying water table. Interestingly, the CH_4 observations presented measured in a wet area of the Horstermeer site were more than double the measurements measured in dry areas of the Horstermeer between 2004 and 2006 using the manual chamber technique (Hendriks et al., 2007). The different chamber measurement locations used by the two studies may account for some of the observed differences. Heterogeneous vegetation and heterogeneous water levels relative to the surface are known to impact both automated and manual flux chamber measurements. For this reason, observational measurements are impacted by the physical placement of flux chambers in the field, leading to potential measurement bias (Speckman et al., 2015; Baldocchi, 2003). At very heterogeneous sites, such as the Horstermeer site, flux strengths vary due to micro-topography (Wania et al., 2010), and chamber measurements have been reported to vary significantly within one site, which may explain differences between studies.

The Horstermeer site has vegetation standing taller than 1 m. At times, it was necessary to consider the vegetation height when selecting the chamber location to ensure vegetation (even when folded) could fit within measurement chambers. Field measurements that exclude areas covered by tall vegetation may result in a significant underestimation of CO_2 or, particularly, CH_4 fluxes. The absence of tall-vegetation measurements limits the capacity to test model representations of tall-vegetation processes, restricting the ability to predict changes in CO_2 and CH_4 fluxes in the presence of tall vegetation (Pangala et al., 2013). Due to the labour-intensive nature of accumulating chamber observations consistently through time, these observational datasets do not offer complete temporal continuity, creating an intermittency bias. The high cost of AC meant that sites could not be measured

simultaneously, leading to an interrupted sampling regime that may bias CO_2 and CH_4 flux estimates (Morin et al., 2014a, 2017). Most chamber measurements are taken during the plant-growing season, assuming that the winter fluxes are negligible, which has been shown to not always be the case (Morin et al., 2014b). Future studies can benefit from continuous AC measurements.

4.1.3 On the efficacy of simulating dynamic vegetation

The PVN model was developed by building upon the functionality and structure of the Peatland-VU model whilst incorporating vegetation dynamics from the NUCOM model. The model has incorporated vegetation dynamics and enhanced the Peatland-VU model's existing carbon-cycling processes. Competition is based on water table depth, temperature, vegetation height, and shading. To verify that the model dynamics are robust and to understand the sensitivity of the PFTs, we performed model sensitivity simulations.

Considering that the short grass, *Sphagnum*, and brown moss PFTs share similar PFT parameters, these three PFTs can respond somewhat similarly. Whilst the short grass PFT is a non-moss PFT, its parameters are not dissimilar to those of moss PFTs. However, the short grass PFT quickly increases in biomass due to its broad range of temperatures and water levels for growth. This means that the short grass PFT provides strong competition against other PFTs. Even though the short grass PFT is height limited, its quickly increasing biomass allows increasing access to PAR, which leads to large amounts of plant respiration, root growth, and net CO_2 fluxes when compared to the *Sphagnum* and brown moss PFTs. With only a shallow root system (maximum 0.1 m), moss PFTs have limited abilities to transport belowground CO_2, and, as expected, the total belowground CO_2 flux is small for mosses. Whilst mosses do not have root structures in reality, we allocated moss PFTs to have a presence in the top 10 cm of the soil layer because, in the presence of bryophytes, there is often no clear separation between the living-moss layer and the soil surface. In this way, we intended to replicate a transition zone. Key differences in the parameters between short grasses and brown mosses are that short grasses are not considered to be a moss PFT (relevant for height growth and light interception). In the model, moss PFTs have large CH_4 vP values and low leaf maintenance respiration coefficients and biomass senescence values (Table 1). Whilst these differentiations have been somewhat effective, future model versions might consider further ways of distinguishing moss PFTs (especially *Sphagnum*). The presence of *Sphagnum* in SOM increases the acidity of the soil. By influencing the acidity of the soil and limiting the nutrient availability, *Sphagnum* gains an advantage over other plant types because *Sphagnum* flourishes in nutrient-poor conditions (Moore et al., 2007). A useful addition to future model versions may be to adapt the living-moss layer to be incorporated into the soil layer, altering the height of the land sur-

face and simulating hummock and hollow microtopography, as well as impacting corresponding soil properties (e.g. pH, DBD).

Largely, decomposition of the peat reservoir led to enhanced CO_2 fluxes due to a thick aerobic layer with low water levels. Modelled photosynthesis and plant respiration are dependent on both temperature and water levels. This enables an assessment of the impacts of water availability and extreme temperatures on plant type. Future model applications may consider the relationship between water availability and plant dynamics and, particularly, the impacts of drought on plant photosynthetic capacity, respiration, soil respiration, and CH_4 production and oxidation.

4.1.4 Impacts of changing temperature input

Studies show that, whilst both CH_4 production and oxidation rates are enhanced by warming, the net CH_4 flux increases with warming because CH_4 production increases at a rate faster than oxidation (Granberg et al., 1999). As expected, the PVN model simulated enhanced CH_4 emissions under simulations driven by warmer temperatures and simulated reduced CH_4 emissions under simulations driven by cooler temperatures. *Sphagnum*, tall grasses, and brown mosses showed unexpected results because they released fewer CH_4 emissions under warmer simulations. This may be indicative of the narrow temperature limits of *Sphagnum* moss (Gunnarsson et al., 2004). The impacts of temperature on model processes are 3-fold. Firstly, the amounts of photosynthesis and plant respiration performed are dependent on the ideal and tolerated PFT growth temperatures. Secondly, the amount of litter converted to belowground SOM reservoirs is dependent on soil temperatures, where warmer soil temperatures lead to larger amounts of litter being converted to belowground reservoirs. Thirdly, decomposition of belowground SOM is dependent on soil layer temperature (as well as pH, saturation, etc.), where soil layers closer to the surface are warmer. Thereby, temperature influences the PFT abundance, the size of litter, and the belowground SOM reservoirs available for decomposition, along with the efficiency of belowground SOM decomposition in the model. The results of our sensitivity analyses are in agreement with field studies which have found that CH_4 emissions are typically higher when dominated by *Carex* compared to *Eriophorum* or *Juncus* (Ström et al., 2005; Jackowicz-Korczyński et al., 2010). This is likely partly due to the presence of aerenchyma and partly due to differing litter quality and rates of carbon turnover (Christensen et al., 2003; Ström et al., 2015).

4.1.5 Belowground decomposition

Enabling different PFTs to contribute to, oxidise, and decompose different belowground SOM pools impacted simulated CO_2 and CH_4 fluxes. Decomposition in the PVN model is dependent on the decomposition rates of different

PFTs. Decomposition rates have been found to differ between forbs, graminoids, deciduous shrubs, and evergreen shrubs (Dorrepaal et al., 2006, 2007, 2009). The peat SOM pool of moss PFTs contributes to CO_2 and CH_4 fluxes because (*Sphagnum*) mosses are the primary peat-contributing plant, and mosses (especially *Sphagnum*) have slow decomposition rates (Hobbie et al., 2000). Moss PFTs are the only PFTs able to contribute to the peat SOM pool, which means that the CH_4 fluxes arising from decomposition of the peat SOM pool are only transferred to the surface by moss PFTs. Future modelling efforts could work to improve the representation of peat decomposition, whereby CO_2 fluxes resulting from the decomposition of peat can be transferred to the surface by both moss and non-moss PFTs. Mosses are prescribed to have roots of 0.1 m at maximum the model is initialised, and this remains constant throughout the model simulation. Mosses do not have an aboveground litter layer, and instead, their living biomass after senescence is added directly to the belowground SOM.

4.1.6 Root distribution representation

Plant-transported CH_4 and aerobic CO_2 production processes are dependent on root mass and are independent of aboveground biomass. In the model, the belowground CO_2 flux is comprised of CO_2 produced by peat, root exudates, litter, roots, microbial biomass, humic matter, and CH_4 oxidation. Root traits play an important role in species competition and processes such as leaf : root allocation, turnover, root stocks, and root distributions have been shown to be dependent on climate, species, and land cover type (Smithwick et al., 2014), particularly in Arctic and boreal systems (Iversen et al., 2015). Root exudation plays an important role in the supply of substrates that can later be metabolised into CH_4 (Aulakh et al., 2001; Waldo et al., 2019), where the fraction of belowground production that consists of exudates (REX) was an important parameter impacting CH_4 production in the model. Next to this, the parameter representing root aerenchyma (PlOx) played a role in the oxidation of CH_4 (Walter and Heimann, 2000). These processes, as well as plant-transported CH_4, are only possible from soil layers with roots present (Bansal et al., 2020; Walter and Heimann, 2000). For this reason, the parameter representing maximum root depth (MRD) played a role in the production, oxidation, and transport of CH_4, where the relative impact of each of these processes on surface CH_4 fluxes is dependent on PFT properties.

Root distribution structural representation is important to reliably simulate CO_2 and CH_4 fluxes in the model. Land surface models have, for the most part, used exponential relationships to describe root distribution (Smithwick et al., 2014; Zeng, 2001). Advances have been made in developing the knowledge and observational data of root distributions in boreal peatland systems. Whilst the exponential relationship is representative for several peatland plant types, an alternative root representation for the exponential relationship may be relevant for certain peatland plant types (Clemmensen et al., 2013; Iversen et al., 2015). Future model versions may consider introducing alternative root representations.

4.1.7 The impact of harvests on plant competition

The inclusion of harvest has proven to be necessary to reproduce the seasonal variability of emissions in grasslands and croplands, where crop harvests occur (Van den Hoof et al., 2011). Whilst CO_2 emissions were reduced with increased harvest frequency, these emissions do not consider off-site decomposition of harvested biomass. The harvest method implemented in the PVN model was similar to the instantaneous harvest method featured in other dynamic vegetation models (such as JULES, Littleton et al. (2020)), where the plant is reduced to a certain set height, and living biomass and LAI are subsequently adjusted accordingly. JULES assumes that 100 % of lost biomass is harvested whilst killing off a proportion of belowground biomass that is converted to litter. The PVN model assumes that 20 % of harvested biomass is lost to litter and does not account for root death. The increased litter layer leads to enhanced emissions resulting from the decomposition of the litter layer. The PFT living biomass is reduced by the proportional biomass lost, assuming the plant's biomass is uniformly distributed with height, and LAI is recalculated. Root mass observational measurements over time, as well as observational data on the impact of harvests on plant productivity, would further improve model representations of harvests. A further assessment may investigate in what ways the photosynthesising and gas conduit capacities of plants are further reduced in the days after harvest and how this can be better captured by the model.

4.2 Comparison to other site-specific peatland GHG emission models

Here, we compare the functionality of the new PVN model against its parent models, the Peatland-VU and NUCOM-BOG models. We then also compare the functionality of the PVN model against the functionality of PEATBOG, the one other site-specific peatland GHG emissions model that includes dynamic vegetation (Table S1). We have developed a new model capable of understanding the role dynamic PFTs play in CO_2 and CH_4 emissions in peatlands. The PVN model simulation results estimated the 1995–2017 annually averaged net GHG budget to be larger than that of the Peatland-VU model at both sites. We suspect that there are two reasons for this, the first being a trade-off between enhanced CO_2 emissions or enhanced CH_4 emissions. In both the Peatland-VU and PVN models, the CO_2 processes are calculated first. Calibration of the photosynthesis- and plant-respiration-related parameters impacts the amount of CO_2 available for CH_4 production. Photosynthesis and leaf respiration mechanisms were the greatest cause of uncertainty

in the model's ability to reproduce the net GHG budget. Future model versions may consider ways to constrain the net CO_2 flux by improving the response of photosynthesis to environmental variables. To improve upon this in future model versions, it may be useful to consider the representation of belowground carbon decomposition. The belowground CH_4 pool in the Peatland-VU model increased consistently during the model simulation; therefore, an increasing quantity of CH_4 was released from the soil profile throughout the simulation, indicating that these fluxes were likely underestimated early in the simulation. The PVN model prescribes each PFT to have root and shoot mass and root depths. This enables each PFT to access different soil layers and belowground CH_4 and carbon pools, potentially impacting the long-term variability of CH_4 emissions. When compared to observed fluxes, the results indicated that the CO_2 scheme in the PVN model may have limited skill when applied to peatland sites of certain physical properties. These results cannot be compared with previous modelling studies because the Peatland-VU CO_2 production scheme results have not been published since the CO_2 production scheme was introduced by Mi et al. (2014) for assessment of the impact on simulated CH_4 fluxes.

The NUCOM model was developed to assess the impact of climate change on bog ecosystems by analysing simulations lasting 200–500 years. Running the model over time periods similar to the NUCOM's 1760–2000 simulation period can be used to assess the model's ability to reproduce shifts in vegetation in response to climate variability. This would require model evaluation using multi-centennial observational data, such as macrofossil evidence. To further investigate the impact of climate change on peatland ecosystems, future studies may consider using macrofossil data in combination with forward or backward multi-decadal or multi-centennial climate projections.

The PEATBOG model (Wu and Blodau, 2013) is the one other site-specific peatland model that simulates CO_2 and CH_4 fluxes and includes competition between moss, shrub, and graminoid PFTs. The PEATBOG model has simulated the Mer Bleue bog in Canada, a pristine (untouched) raised acidic ombrotrophic bog, over a 6-year period. The Mer Bleue bog is a nutrient-poor bog unlike the two sites assessed in this study. The net annual GHG emissions for the Mer Bleue bog site were small, approximately 0.02 % of the GHG emissions observed at the Ilperveld field site in the Netherlands. Peat has been accumulating at this site since 8400 cal yr BP and has developed a peat depth of 6 m in the centre. The PEATBOG model is a complex model that simulates many of the same processes as the PVN model but beyond this also includes representation of the nitrogen cycling, electron-accepting processes, dissolved inorganic and organic carbon, and subsequent CO_2 and CH_4 run-off. The PEATBOG model underestimated the annual net GHG emissions (net ecosystem carbon balance) by approximately half of observed field observations. Wu and Blodau (2013) noted the sensitivity of the PEATBOG model to temperature, re-

porting that $1 \, °C$ of temperature change was enough to initiate a model bias, swaying the model from a source to a sink. This is concurrent with the results of the sensitivity testing performed in this study, which showed that changes in air temperature had large impacts on both CO_2 and CH_4 emissions. Plot-scale model inter-comparison efforts could help improve the representation of small-scale processes in peatland models. However, the breadth of observational data required to run and test site-specific models makes site-specific model inter-comparison efforts cumbersome and difficult.

5 Conclusions

Here, we present Peatland-VU-NUCOM v1.0 (PVN), a new site-specific peatland dynamic vegetation emissions model. By including plant–environmental feedbacks, the model can serve wetland management by estimating changes in the GHG balance of peatland sites in response to environmental changes – such as changing air temperatures, water levels, or precipitation and/or evapotranspiration – or new management decisions – such as raising the water table, vegetation restoration, or modifying mowing regimes. The PVN model was designed to simulate plant competition above- and belowground whilst developing carbon pools for the production and oxidation of CH_4 and CO_2. PFTs compete for light where production and respiration are dependent on ideal temperature and water levels. Structural differences in vegetation root, exudation, and stem representation impact CH_4 production, oxidation, and transport. Peatlands are one of the most important carbon-storing ecosystems. The challenges facing our understanding of the carbon balance and CH_4 dynamics subsequent to the rewetting of previously managed peatlands are numerous. One challenge is the ability of site-specific peatland models to reproduce CH_4 fluxes, particularly in relation to plant functioning. This question is particularly timely because there exists an urgent need to restore drained peatlands to reduce land subsidence whilst limiting GHG emissions. We show that the PVN model is able to reproduce plant biomass fractions and CH_4 and CO_2 fluxes under changing environmental conditions. This confirms that the model provides the capability to understand the relationship between peatland plant dynamics and CH_4 and CO_2 emissions. The PVN model is a relevant tool that can be used to optimise vegetation management with the goal of reducing GHG emissions.

eterisations, site soil profiles, climate data, water level data, and PFTs. The exact version of the model source code used to produce the results presented in this paper is archived on Zenodo (https://doi.org/10.5281/zenodo.7701698, Lippmann and van Huissteden (2023)).

Supplement. The supplement related to this article is available online at: https://doi.org/10.5194/gmd-16-6773-2023-supplement.

References

Alhoz, K., Kenesei, K., Papageorgiou, M., Keurentjes, E. E. M., and de Jong, M.: Improved AHN3 Gridded DTM/DSM, Delft University of Technology, https://repository.tudelft.nl/islandora/object/uuid:153b2a82-05ba-412b-8a0a-119cb5689afd (last access: 15 November 2023) 2020.

Aulakh, M. S., Wassmann, R., Bueno, C., and Rennenberg, H.: Impact of root exudates of different cultivars and plant development stages of rice (Oryza sativa L.) on methane production in a paddy soil, Plant Soil, 230, 77–86, https://doi.org/10.1023/A:1004817212321, 2001.

Baldocchi, D. D.: Assessing the eddy covariance technique for evaluating carbon dioxide exchange rates of ecosystems: Past, present and future, Glob. Change Biol., 9, 479–492, https://doi.org/10.1046/j.1365-2486.2003.00629.x, 2003.

Baldocchi, D. D. and Harley, P. C.: Scaling carbon dioxide and water vapour exchange from leaf to canopy in a deciduous forest. II. Model testing and application, Plant Cell Environ., 18, 1157–1173, https://doi.org/10.1111/j.1365-3040.1995.tb00626.x, 1995.

Ballantyne, D. M., Hribljan, J. A., Pypker, T. G., and Chimner, R. A.: Long-term water table manipulations alter peatland gaseous carbon fluxes in Northern Michigan, Wetl. Ecol. Manag., 22, 35–47, https://doi.org/10.1007/s11273-013-9320-8, 2014.

Bansal, S., Johnson, O. F., Meier, J., and Zhu, X.: Vegetation Affects Timing and Location of Wetland Methane Emissions, J. Geophys. Res.-Biogeo., 125, e2020JG005777, https://doi.org/10.1029/2020JG005777, 2020.

Bao, T., Jia, G., and Xu, X.: Weakening greenhouse gas sink of pristine wetlands under warming, Nat. Clim. Change, 13, 462–469, https://doi.org/10.1038/s41558-023-01637-0, 2023.

Basile-Doelsch, I., Balesdent, J., and Pellerin, S.: Reviews and syntheses: The mechanisms underlying carbon storage in soil, Biogeosciences, 17, 5223–5242, https://doi.org/10.5194/bg-17-5223-2020, 2020.

Beven, K. and Freer, J.: Equifinality, data assimilation, and uncertainty estimation in mechanistic modelling of complex environmental systems using the GLUE methodology, J. Hydrol., 249, 11–29, https://doi.org/10.1016/S0022-1694(01)00421-8, 2001.

Boonman, J., Hefting, M. M., van Huissteden, C. J. A., van den Berg, M., van Huissteden, J. (., Erkens, G., Melman, R., and van der Velde, Y.: Cutting peatland CO2 emissions with water management practices, Biogeosciences, 19, 5707–5727, https://doi.org/10.5194/bg-19-5707-2022, 2022.

Box, J. E., Colgan, W. T., Christensen, T. R., Schmidt, N. M., Lund, M., Parmentier, F. J. W., Brown, R., Bhatt, U. S., Euskirchen, E. S., Romanovsky, V. E., Walsh, J. E., Overland, J. E., Wang, M., Corell, R. W., Meier, W. N., Wouters, B., Mernild, S., Mård, J., Pawlak, J., and Olsen, M. S.: Key indicators of Arctic climate change: 1971-2017, Environ. Res. Lett., 14, 045010, https://doi.org/10.1088/1748-9326/aafc1b, 2019.

Bridgham, S. D., Cadillo-Quiroz, H., Keller, J. K., and Zhuang, Q.: Methane emissions from wetlands: Biogeochemical, microbial, and modeling perspectives from local to global scales, Glob. Change Biol., 19, 1325–1346, https://doi.org/10.1111/gcb.12131, 2013.

Bubier, J.: The Relationship of Vegetation to Methane Emission and Hydrochemical Gradients in Northern Peatlands, J. Ecol., 83, 403–420, 2016.

Chaney, N. W., Sheffield, J., Villarini, G., and Wood, E. F.: Development of a high-resolution gridded daily meteorological dataset over sub-Saharan Africa: Spatial analysis of trends in climate extremes, J. Climate, 27, 5815–5835, https://doi.org/10.1175/JCLI-D-13-00423.1, 2014.

Christensen, T. R., Ekberg, A., Ström, L., Mastepanov, M., Panikov, N., Öquist, M., Svensson, B. H., Nykänen, H., Martikainen, P. J., and Oskarsson, H.: Factors controlling large scale variations in methane emissions from wetlands, Geophys. Res. Lett., 30, 67, https://doi.org/10.1029/2002GL016848, 2003.

Churkina, G., Running, S. W., and Schloss, A. L.: Comparing global models of terrestrial net primary productivity (NPP): The importance of water availability, Glob. Change Biol., 5, 46–55, https://doi.org/10.1046/j.1365-2486.1999.00006.x, 1999.

Clemmensen, K. E., Bahr, A., Ovaskainen, O., Dahlberg, A., Ekblad, A., Wallander, H., Stenlid, J., Finlay, R. D., Wardle, D. A., and Lindahl, B. D.: Roots and Associated Fungi Drive Long-Term Carbon Sequestration in Boreal Forest, Science, 339, 1615–1618, https://doi.org/10.1126/science.1231923, 2013.

Crow, S. E. and Wieder, R. K.: Sources of CO2 emission from a northern peatland: Root respiration, exudation, and decomposition, Ecology, 86, 1825–1834, https://doi.org/10.1890/04-1575, 2005.

Davidson, E. and Janssens, I. A.: Temperature sensitivity of soil carbon decomposition and feedbacks to climate change, Nature, 440, 165–173, https://doi.org/10.1038/nature04514, 2006.

De Boeck, H. J., Dreesen, F. E., Janssens, I. A., and Nijs, I.: Whole-system responses of experimental plant communities to climate extremes imposed in different seasons, New Phytol., 189, 806–817, https://doi.org/10.1111/j.1469-8137.2010.03515.x, 2011.

De La Motte, L. G., Beauclaire, Q., Heinesch, B., Cuntz, M., Foltýnová, L., Šigut, L., Kowalska, N., Manca, G., Ballarin, I. G., Vincke, C., Roland, M., Ibrom, A., Lousteau, D., Siebicke, L., Neiryink, J., and Longdoz, B.: Non-stomatal processes reduce gross primary productivity in temperate forest ecosystems during severe edaphic drought: Edaphic drought in forest ecosystems, Philos. T. Roy. Soc. B, 375, 20190527, https://doi.org/10.1098/rstb.2019.0527, 2020.

De Lange, W. J., Prinsen, G. F., Hoogewoud, J. C., Veldhuizen, A. A., Verkaik, J., Oude Essink, G. H., Van Walsum, P. E., Delsman, J. R., Hunink, J. C., Massop, H. T. L., and Kroon, T.: An operational, multi-scale, multi-model system for consensus-based, integrated water management and policy analysis: The Netherlands Hydrological Instrument, Environ. Model. Softw., 59, 98–108, https://doi.org/10.1016/j.envsoft.2014.05.009, 2014.

Dick, J. J., Tetzlaff, D., Birkel, C., and Soulsby, C.: Modelling landscape controls on dissolved organic carbon sources and fluxes to streams, Biogeochemistry, 122, 361–374, https://doi.org/10.1007/s10533-014-0046-3, 2015.

Dorrepaal, E., Aerts, R., Cornelissen, J. H., Van Logtestijn, R. S., and Callaghan, T. V.: Sphagnum modifies climate-change impacts on subarctic vascular bog plants, Funct. Ecol., 20, 31–41, https://doi.org/10.1111/j.1365-2435.2006.01076.x, 2006.

Dorrepaal, E., Cornelissen, J. H., and Aerts, R.: Changing leaf litter feedbacks on plant production across contrasting sub-arctic peatland species and growth forms, Oecologia, 151, 251–261, https://doi.org/10.1007/s00442-006-0580-3, 2007.

Dorrepaal, E., Toet, S., Van Logtestijn, R. S., Swart, E., Van De Weg, M. J., Callaghan, T. V., and Aerts, R.: Carbon respiration from subsurface peat accelerated by climate warming in the subarctic, Nature, 460, 616–619, https://doi.org/10.1038/nature08216, 2009.

Erkens, G., Van Der Meulen, M. J., and Middelkoop, H.: Double trouble: Subsidence and CO_2 respiration due to 1,000 years of

Dutch coastal peatlands cultivation, Hydrogeol. J., 24, 551–568, https://doi.org/10.1007/s10040-016-1380-4, 2016.

Evans, C. D., Peacock, M., Baird, A. J., Artz, R. R., Burden, A., Callaghan, N., Chapman, P. J., Cooper, H. M., Coyle, M., Craig, E., Cumming, A., Dixon, S., Gauci, V., Grayson, R. P., Helfter, C., Heppell, C. M., Holden, J., Jones, D. L., Kaduk, J., Levy, P., Matthews, R., McNamara, N. P., Misselbrook, T., Oakley, S., Page, S. E., Rayment, M., Ridley, L. M., Stanley, K. M., Williamson, J. L., Worrall, F., and Morrison, R.: Overriding water table control on managed peatland greenhouse gas emissions, Nature, 593, 548–552, https://doi.org/10.1038/s41586-021-03523-1, 2021.

Frolking, S. and Roulet, N. T.: Holocene radiative forcing impact of northern peatland carbon accumulation and methane emissions, Glob. Change Biol., 13, 1079–1088, https://doi.org/10.1111/j.1365-2486.2007.01339.x, 2007.

Gerten, D., Schaphoff, S., Haberlandt, U., Lucht, W., and Sitch, S.: Terrestrial vegetation and water balance – Hydrological evaluation of a dynamic global vegetation model, J. Hydrol., 286, 249–270, https://doi.org/10.1016/j.jhydrol.2003.09.029, 2004.

Geurts, J. and Fritz, C.: Paludiculture pilots and experiments with focus on cattail and reed in the Netherlands. Technical, Tech. rep., Radboud University Nijmegen, Nijmegen, https://doi.org/10.13140/RG.2.2.12916.24966, 2018.

Gorham, E.: Shoot height, weight and standing crop in relation to density of monospecific plant stands, Nature, 279, 148–150, https://doi.org/10.1038/279148a0, 1979.

Graf, M. and Rochefort, L.: Examining the peat-accumulating potential of fen vegetation in the context of fen restoration of harvested peatlands, Ecoscience, 16, 158–166, https://doi.org/10.2980/16-2-3128, 2009.

Granberg, G., Grip, H., Ottosson Löfvenius, M., Sundh, I., Svensson, B. H., and Nilsson, M.: A simple model for simulation of water content, soil frost, and soil temperatures in boreal mixed mires, Water Resour. Res., 35, 3771–3782, https://doi.org/10.1029/1999WR900216, 1999.

Gunnarsson, U., Granberg, G., and Nilsson, M.: Growth, production and interspecific competition in Sphagnum: Effects of temperature, nitrogen and sulphur treatments on a boreal mire, New Phytol., 163, 349–359, https://doi.org/10.1111/j.1469-8137.2004.01108.x, 2004.

Günther, A., Barthelmes, A., Huth, V., Joosten, H., Jurasinski, G., Koebsch, F., and Couwenberg, J.: Prompt rewetting of drained peatlands reduces climate warming despite methane emissions, Nat. Commun., 11, 1644, https://doi.org/10.1038/s41467-020-15499-z, 2020.

Gupta, H. V., Kling, H., Yilmaz, K. K., and Martinez, G. F.: Decomposition of the mean squared error and NSE performance criteria: Implications for improving hydrological modelling, J. Hydrol., 377, 80–91, https://doi.org/10.1016/j.jhydrol.2009.08.003, 2009.

Harpenslager, S. F., van den Elzen, E., Kox, M. A., Smolders, A. J., Ettwig, K. F., and Lamers, L. P.: Rewetting former agricultural peatlands: Topsoil removal as a prerequisite to avoid strong nutrient and greenhouse gas emissions, Ecol. Eng., 84, 159–168, https://doi.org/10.1016/j.ecoleng.2015.08.002, 2015.

Haxeltine, A. and Prentice, I. C.: BIOME3: An equilibrium terrestrial biosphere model based on ecophysiological constraints, resource availability, and competition among plant

functional types, Global Biogeochem. Cy., 10, 693–709, https://doi.org/10.1029/96GB02344, 1996.

Heijmans, M. M., Mauquoy, D., Van Geel, B., and Berendse, F.: Long-term effects of climate change on vegetation and carbon dynamics in peat bogs, J. Veg. Sci., 19, 307–320, https://doi.org/10.3170/2008-8-18368, 2008.

Heijmans, M. M., Mauquoy, D., Van Geel, B., and Berendse, F.: Long-term effects of climate change on vegetation and carbon dynamics in peat bogs, J. Veg. Sci., 19, 307–320, https://doi.org/10.3170/2008-8-18368, 2008.

Hendriks, D. M. D., van Huissteden, J., Dolman, A. J., and van der Molen, M. K.: The full greenhouse gas balance of an abandoned peat meadow, Biogeosciences, 4, 411–424, https://doi.org/10.5194/bg-4-411-2007, 2007.

Hobbie, S. E., Schimel, J. P., Trumbore, S. E., and Randerson, J. R.: Controls over carbon storage and turnover in high-latitude soils, Glob. Change Biol., 6, 196–210, https://doi.org/10.1046/j.1365-2486.2000.06021.x, 2000.

Högberg, P., Nordgren, A., Buchmann, N., Taylor, A. F., Ekblad, A., Högberg, M. N., Nyberg, G., Ottosson-Löfvenius, M., and Read, D. J.: Large-scale forest girdling shows that current photosynthesis drives soil respiration, Nature, 411, 789–792, https://doi.org/10.1038/35081058, 2001.

Huang, S., Titus, S. J., and Wiens, D. P.: Comparison of nonlinear height-diameter functions for major Alberta tree species, Can. J. Forest Res., 22, 1297–1304, https://doi.org/10.1139/x92-172, 1992.

Iversen, C. M., Sloan, V. L., Sullivan, P. F., Euskirchen, E. S., Mcguire, A. D., Norby, R. J., Walker, A. P., Warren, J. M., and Wullschleger, S. D.: The unseen iceberg: Plant roots in arctic tundra, New Phytol., 205, 34–58, https://doi.org/10.1111/nph.13003, 2015.

Jaatinen, K., Laiho, R., Vuorenmaa, A., Del Castillo, U., Minkkinen, K., Pennanen, T., Penttilä, T., and Fritze, H.: Responses of aerobic microbial communities and soil respiration to water-level drawdown in a northern boreal fen, Environ. Microbiol., 10, 339–353, https://doi.org/10.1111/j.1462-2920.2007.01455.x, 2008.

Jackowicz-Korczyński, M., Christensen, T. R., Bäckstrand, K., Crill, P., Friborg, T., Mastepanov, M., and Ström, L.: Annual cycle of methane emission from a subarctic peatland, J. Geophys. Res.-Biogeo., 115, G02009, https://doi.org/10.1029/2008JG000913, 2010.

Jackson, R. B., Canadell, J., Ehleringer, J. R., Mooney, H. A., Sala, O. E., and Schulze, E. D.: A global analysis of root distributions for terrestrial biomes, Oecologia, 108, 389–411, https://doi.org/10.1007/BF00333714, 1996.

Järveoja, J., Laht, J., Maddison, M., Soosaar, K., Ostonen, I., and Mander, Ü.: Mitigation of greenhouse gas emissions from an abandoned Baltic peat extraction area by growing reed canary grass: Life-cycle assessment, Reg. Environ. Change, 13, 781–795, https://doi.org/10.1007/s10113-012-0355-9, 2013.

Kattge, J., Díaz, S., Lavorel, S., Prentice, I. C., Leadley, P., Bönisch, G., Garnier, E., Westoby, M., Reich, P. B., Wright, I. J., Cornelissen, J. H., Violle, C., Harrison, S. P., Van Bodegom, P. M., Reichstein, M., Enquist, B. J., Soudzilovskaia, N. A., Ackerly, D. D., Anand, M., Atkin, O., Bahn, M., Baker, T. R., Baldocchi, D., Bekker, R., Blanco, C. C., Blonder, B., Bond, W. J., Bradstock, R., Bunker, D. E., Casanoves, F., Cavender-Bares, J., Chambers, J. Q., Chapin, F. S., Chave, J., Coomes, D., Corn-

well, W. K., Craine, J. M., Dobrin, B. H., Duarte, L., Durka, W., Elser, J., Esser, G., Estiarte, M., Fagan, W. F., Fang, J., Fernández-Méndez, F., Fidelis, A., Finegan, B., Flores, O., Ford, H., Frank, D., Freschet, G. T., Fyllas, N. M., Gallagher, R. V., Green, W. A., Gutierrez, A. G., Hickler, T., Higgins, S. I., Hodgson, J. G., Jalili, A., Jansen, S., Joly, C. A., Kerkhoff, A. J., Kirkup, D., Kitajima, K., Kleyer, M., Klotz, S., Knops, J. M., Kramer, K., Kühn, I., Kurokawa, H., Laughlin, D., Lee, T. D., Leishman, M., Lens, F., Lenz, T., Lewis, S. L., Lloyd, J., Llusià, J., Louault, F., Ma, S., Mahecha, M. D., Manning, P., Massad, T., Medlyn, B. E., Messier, J., Moles, A. T., Müller, S. C., Nadrowski, K., Naeem, S., Niinemets, Ü., Nöllert, S., Nüske, A., Ogaya, R., Oleksyn, J., Onipchenko, V. G., Onoda, Y., Ordoñez, J., Overbeck, G., Ozinga, W. A., Patiño, S., Paula, S., Pausas, J. G., Peñuelas, J., Phillips, O. L., Pillar, V., Poorter, H., Poorter, L., Poschlod, P., Prinzing, A., Proulx, R., Rammig, A., Reinsch, S., Reu, B., Sack, L., Salgado-Negret, B., Sardans, J., Shiodera, S., Shipley, B., Siefert, A., Sosinski, E., Soussana, J. F., Swaine, E., Swenson, N., Thompson, K., Thornton, P., Waldram, M., Weiher, E., White, M., White, S., Wright, S. J., Yguel, B., Zaehle, S., Zanne, A. E., and Wirth, C.: TRY – a global database of plant traits, Glob. Change Biol., 17, 2905–2935, https://doi.org/10.1111/j.1365-2486.2011.02451.x, 2011.

Kattge, J., Bönisch, G., Díaz, S., Lavorel, S., Prentice, I. C., Leadley, P., Tautenhahn, S., Werner, G. D., Aakala, T., Abedi, M., Acosta, A. T., Adamidis, G. C., Adamson, K., Aiba, M., Albert, C. H., Alcántara, J. M., Alcázar C, C., Aleixo, I., Ali, H., Amiaud, B., Ammer, C., Amoroso, M. M., Anand, M., Anderson, C., Anten, N., Antos, J., Apgaua, D. M. G., Ashman, T. L., Asmara, D. H., Asner, G. P., Aspinwall, M., Atkin, O., Aubin, I., Baastrup-Spohr, L., Bahalkeh, K., Bahn, M., Baker, T., Baker, W. J., Bakker, J. P., Baldocchi, D., Baltzer, J., Banerjee, A., Baranger, A., Barlow, J., Barneche, D. R., Baruch, Z., Bastianelli, D., Battles, J., Bauerle, W., Bauters, M., Bazzato, E., Beckmann, M., Beeckman, H., Beierkuhnlein, C., Bekker, R., Belfry, G., Belluau, M., Beloiu, M., Benavides, R., Benomar, L., Berdugo-Lattke, M. L., Berenguer, E., Bergamin, R., Bergmann, J., Bergmann Carlucci, M., Berner, L., Bernhardt-Römermann, M., Bigler, C., Bjorkman, A. D., Blackman, C., Blanco, C., Blonder, B., Blumenthal, D., Bocanegra-González, K. T., Boeckx, P., Bohlman, S., Böhning-Gaese, K., Boisvert-Marsh, L., Bond, W., Bond-Lamberty, B., Boom, A., Boonman, C. C., Bordin, K., Boughton, E. H., Boukili, V., Bowman, D. M., Bravo, S., Brendel, M. R., Broadley, M. R., Brown, K. A., Bruelheide, H., Brumnich, F., Bruun, H. H., Bruy, D., Buchanan, S. W., Bucher, S. F., Buchmann, N., Buitenwerf, R., Bunker, D. E., Bürger, J., Burrascano, S., Burslem, D. F., Butterfield, B. J., Byun, C., Marques, M., Scalon, M. C., Caccianiga, M., Cadotte, M., Cailleret, M., Camac, J., Camarero, J. J., Campany, C., Campetella, G., Campos, J. A., Cano-Arboleda, L., Canullo, R., Carbognani, M., Carvalho, F., Casanoves, F., Castagneyrol, B., Catford, J. A., Cavender-Bares, J., Cerabolini, B. E., Cervellini, M., Chacón-Madrigal, E., Chapin, K., Chapin, F. S., Chelli, S., Chen, S. C., Chen, A., Cherubini, P., Chianucci, F., Choat, B., Chung, K. S., Chytrý, M., Ciccarelli, D., Coll, L., Collins, C. G., Conti, L., Coomes, D., Cornelissen, J. H., Cornwell, W. K., Corona, P., Coyea, M., Craine, J., Craven, D., Cromsigt, J. P., Csecserits, A., Cufar, K., Cuntz, M., da Silva, A. C., Dahlin, K. M., Dainese, M., Dalke, I., Dalle Fratte, M., Dang-Le, A. T.,

Danihelka, J., Dannoura, M., Dawson, S., de Beer, A. J., De Frutos, A., De Long, J. R., Dechant, B., Delagrange, S., Delpierre, N., Derroire, G., Dias, A. S., Diaz-Toribio, M. H., Dimitrakopoulos, P. G., Dobrowolski, M., Doktor, D., Dřevojan, P., Dong, N., Dransfield, J., Dressler, S., Duarte, L., Ducouret, E., Dullinger, S., Durka, W., Duursma, R., Dymova, O., E-Vojtkó, A., Eckstein, R. L., Ejtehadi, H., Elser, J., Emilio, T., Engemann, K., Erfanian, M. B., Erfmeier, A., Esquivel-Muelbert, A., Esser, G., Estiarte, M., Domingues, T. F., Fagan, W. F., Fagúndez, J., Falster, D. S., Fan, Y., Fang, J., Farris, E., Fazlioglu, F., Feng, Y., Fernandez-Mendez, F., Ferrara, C., Ferreira, J., Fidelis, A., Finegan, B., Firn, J., Flowers, T. J., Flynn, D. F., Fontana, V., Forey, E., Forgiarini, C., François, L., Frangipani, M., Frank, D., Frenette-Dussault, C., Freschet, G. T., Fry, E. L., Fyllas, N. M., Mazzochini, G. G., Gachet, S., Gallagher, R., Ganade, G., Ganga, F., García-Palacios, P., Gargaglione, V., Garnier, E., Garrido, J. L., de Gasper, A. L., Gea-Izquierdo, G., Gibson, D., Gillison, A. N., Giroldo, A., Glasenhardt, M. C., Gleason, S., Gliesch, M., Goldberg, E., Göldel, B., Gonzalez-Akre, E., Gonzalez-Andujar, J. L., González-Melo, A., González-Robles, A., Graae, B. J., Granda, E., Graves, S., Green, W. A., Gregor, T., Gross, N., Guerin, G. R., Günther, A., Gutiérrez, A. G., Haddock, L., Haines, A., Hall, J., Hambuckers, A., Han, W., Harrison, S. P., Hattingh, W., Hawes, J. E., He, T., He, P., Heberling, J. M., Helm, A., Hempel, S., Hentschel, J., Hérault, B., Hereş, A. M., Herz, K., Heuertz, M., Hickler, T., Hietz, P., Higuchi, P., Hipp, A. L., Hirons, A., Hock, M., Hogan, J. A., Holl, K., Honnay, O., Hornstein, D., Hou, E., Hough-Snee, N., Hovstad, K. A., Ichie, T., Igić, B., Illa, E., Isaac, M., Ishihara, M., Ivanov, L., Ivanova, L., Iversen, C. M., Izquierdo, J., Jackson, R. B., Jackson, B., Jactel, H., Jagodzinski, A. M., Jandt, U., Jansen, S., Jenkins, T., Jentsch, A., Jespersen, J. R. P., Jiang, G. F., Johansen, J. L., Johnson, D., Jokela, E. J., Joly, C. A., Jordan, G. J., Joseph, G. S., Junaedi, D., Junker, R. R., Justes, E., Kabzems, R., Kane, J., Kaplan, Z., Kattenborn, T., Kavelenova, L., Kearsley, E., Kempel, A., Kenzo, T., Kerkhoff, A., Khalil, M. I., Kinlock, N. L., Kissling, W. D., Kitajima, K., Kitzberger, T., Kjøller, R., Klein, T., Kleyer, M., Klimešová, J., Klipel, J., Kloeppel, B., Klotz, S., Knops, J. M., Kohyama, T., Koike, F., Kollmann, J., Komac, B., Komatsu, K., König, C., Kraft, N. J., Kramer, K., Kreft, H., Kühn, I., Kumarathunge, D., Kuppler, J., Kurokawa, H., Kurosawa, Y., Kuyah, S., Laclau, J. P., Lafleur, B., Lallai, E., Lamb, E., Lamprecht, A., Larkin, D. J., Laughlin, D., Le Bagousse-Pinguet, Y., le Maire, G., le Roux, P. C., le Roux, E., Lee, T., Lens, F., Lewis, S. L., Lhotsky, B., Li, Y., Li, X., Lichstein, J. W., Liebergesell, M., Lim, J. Y., Lin, Y. S., Linares, J. C., Liu, C., Liu, D., Liu, U., Livingstone, S., Llusià, J., Lohbeck, M., López-García, Á., Lopez-Gonzalez, G., Lososová, Z., Louault, F., Lukács, B. A., Lukeš, P., Luo, Y., Lussu, M., Ma, S., Maciel Rabelo Pereira, C., Mack, M., Maire, V., Mäkelä, A., Mäkinen, H., Malhado, A. C. M., Mallik, A., Manning, P., Manzoni, S., Marchetti, Z., Marchino, L., Marcilio-Silva, V., Marcon, E., Marignani, M., Markesteijn, L., Martin, A., Martínez-Garza, C., Martínez-Vilalta, J., Mašková, T., Mason, K., Mason, N., Massad, T. J., Masse, J., Mayrose, I., McCarthy, J., McCormack, M. L., McCulloh, K., McFadden, I. R., McGill, B. J., McPartland, M. Y., Medeiros, J. S., Medlyn, B., Meerts, P., Mehrabi, Z., Meir, P., Melo, F. P., Mencuccini, M., Meredieu, C., Messier, J., Mészáros, I., Metsaranta, J., Michaletz, S. T., Michelaki, C., Migalina, S., Milla, R., Miller, J. E., Minden, V., Ming, R., Mokany, K., Moles, A. T., Molnár, A., Molofsky, J., Molz, M., Montgomery, R. A., Monty, A., Moravcová, L., Moreno-Martínez, A., Moretti, M., Mori, A. S., Mori, S., Morris, D., Morrison, J., Mucina, L., Mueller, S., Muir, C. D., Müller, S. C., Munoz, F., Myers-Smith, I. H., Myster, R. W., Nagano, M., Naidu, S., Narayanan, A., Natesan, B., Negoita, L., Nelson, A. S., Neuschulz, E. L., Ni, J., Niedrist, G., Nieto, J., Niinemets, Ü., Nolan, R., Nottebrock, H., Nouvellon, Y., Novakovskiy, A., Nystuen, K. O., O'Grady, A., O'Hara, K., O'Reilly-Nugent, A., Oakley, S., Oberhuber, W., Ohtsuka, T., Oliveira, R., Öllerer, K., Olson, M. E., Onipchenko, V., Onoda, Y., Onstein, R. E., Ordonez, J. C., Osada, N., Ostonen, I., Ottaviani, G., Otto, S., Overbeck, G. E., Ozinga, W. A., Pahl, A. T., Paine, C. E., Pakeman, R. J., Papageorgiou, A. C., Parfionova, E., Pärtel, M., Patacca, M., Paula, S., Paule, J., Pauli, H., Pausas, J. G., Peco, B., Penuelas, J., Perea, A., Peri, P. L., Petisco-Souza, A. C., Petraglia, A., Petritan, A. M., Phillips, O. L., Pierce, S., Pillar, V. D., Pisek, J., Pomogaybin, A., Poorter, H., Portsmuth, A., Poschlod, P., Potvin, C., Pounds, D., Powell, A. S., Power, S. A., Prinzing, A., Puglielli, G., Pyšek, P., Raevel, V., Rammig, A., Ransijn, J., Ray, C. A., Reich, P. B., Reichstein, M., Reid, D. E., Réjou-Méchain, M., de Dios, V. R., Ribeiro, S., Richardson, S., Riibak, K., Rillig, M. C., Riviera, F., Robert, E. M., Roberts, S., Robroek, B., Roddy, A., Rodrigues, A. V., Rogers, A., Rollinson, E., Rolo, V., Römermann, C., Ronzhina, D., Roscher, C., Rosell, J. A., Rosenfield, M. F., Rossi, C., Roy, D. B., Royer-Tardif, S., Rüger, N., Ruiz-Peinado, R., Rumpf, S. B., Rusch, G. M., Ryo, M., Sack, L., Saldaña, A., Salgado-Negret, B., Salguero-Gomez, R., Santa-Regina, I., Santacruz-García, A. C., Santos, J., Sardans, J., Schamp, B., Scherer-Lorenzen, M., Schleuning, M., Schmid, B., Schmidt, M., Schmitt, S., Schneider, J. V., Schowanek, S. D., Schrader, J., Schrodt, F., Schuldt, B., Schurr, F., Selaya Garvizu, G., Semchenko, M., Seymour, C., Sfair, J. C., Sharpe, J. M., Sheppard, C. S., Sheremetiev, S., Shiodera, S., Shipley, B., Shovon, T. A., Siebenkäs, A., Sierra, C., Silva, V., Silva, M., Sitzia, T., Sjöman, H., Slot, M., Smith, N. G., Sodhi, D., Soltis, P., Soltis, D., Somers, B., Sonnier, G., Sørensen, M. V., Sosinski, E. E., Soudzilovskaia, N. A., Souza, A. F., Spasojevic, M., Sperandii, M. G., Stan, A. B., Stegen, J., Steinbauer, K., Stephan, J. G., Sterck, F., Stojanovic, D. B., Strydom, T., Suarez, M. L., Svenning, J. C., Svitková, I., Svitok, M., Svoboda, M., Swaine, E., Swenson, N., Tabarelli, M., Takagi, K., Tappeiner, U., Tarifa, R., Tauugourdeau, S., Tavsanoglu, C., te Beest, M., Tedersoo, L., Thiffault, N., Thom, D., Thomas, E., Thompson, K., Thornton, P. E., Thuiller, W., Tichý, L., Tissue, D., Tjoelker, M. G., Tng, D. Y. P., Tobias, J., Török, P., Tarin, T., Torres-Ruiz, J. M., Tóthmérész, B., Treurnicht, M., Trivellone, V., Trolliet, F., Trotsiuk, V., Tsakalos, J. L., Tsiripidis, I., Tysklind, N., Umehara, T., Usoltsev, V., Vadeboncoeur, M., Vaezi, J., Valladares, F., Vamosi, J., van Bodegom, P. M., van Breugel, M., Van Cleemput, E., van de Weg, M., van der Merwe, S., van der Plas, F., van der Sande, M. T., van Kleunen, M., Van Meerbeek, K., Vanderwel, M., Vanselow, K. A., Vårhammar, A., Varone, L., Vasquez Valderrama, M. Y., Vassilev, K., Vellend, M., Veneklaas, E. J., Verbeeck, H., Verheyen, K., Vibrans, A., Vieira, I., Villacís, J., Violle, C., Vivek, P., Wagner, K., Waldram, M., Waldron, A., Walker, A. P., Waller, M., Walther, G., Wang, H., Wang, F., Wang, W., Watkins, H., Watkins, J., Weber, U., Weedon, J. T., Wei, L., Weigelt, P., Weiher, E., Wells, A. W., Wellstein,

C., Wenk, E., Westoby, M., Westwood, A., White, P. J., Whitten, M., Williams, M., Winkler, D. E., Winter, K., Womack, C., Wright, I. J., Wright, S. J., Wright, J., Pinho, B. X., Ximenes, F., Yamada, T., Yamaji, K., Yanai, R., Yankov, N., Yguel, B., Zanini, K. J., Zanne, A. E., Zelený, D., Zhao, Y. P., Zheng, J., Zheng, J., Ziemińska, K., Zirbel, C. R., Zizka, G., Zo-Bi, I. C., Zotz, G., and Wirth, C.: TRY plant trait database – enhanced coverage and open access, Glob. Change Biol., 26, 119–188, https://doi.org/10.1111/gcb.14904, 2020.

Keenan, T., Sabate, S., and Gracia, C.: The importance of mesophyll conductance in regulating forest ecosystem productivity during drought periods, Glob. Change Biol., 16, 1019–1034, https://doi.org/10.1111/j.1365-2486.2009.02017.x, 2010.

Kling, H., Fuchs, M., and Paulin, M.: Runoff conditions in the upper Danube basin under an ensemble of climate change scenarios, J. Hydrol., 424–425, 264–277, https://doi.org/10.1016/j.jhydrol.2012.01.011, 2012.

Knox, S. H., Sturtevant, C., Matthes, J. H., Koteen, L., Verfaillie, J., and Baldocchi, D.: Agricultural peatland restoration: Effects of land-use change on greenhouse gas (CO_2 and CH_4) fluxes in the Sacramento-San Joaquin Delta, Glob. Change Biol., 21, 750–765, https://doi.org/10.1111/gcb.12745, 2015.

Koebsch, F., Sonnentag, O., Järveoja, J., Peltoniemi, M., Alekseychik, P., Aurela, M., Arslan, A. N., Dinsmore, K., Gianelle, D., Helfter, C., Jackowicz-Korczynski, M., Korrensalo, A., Leith, F., Linkosalmi, M., Lohila, A., Lund, M., Maddison, M., Mammarella, I., Mander, Ü., Minkkinen, K., Pickard, A., Pullens, J. W., Tuittila, E. S., Nilsson, M. B., and Peichl, M.: Refining the role of phenology in regulating gross ecosystem productivity across European peatlands, Glob. Change Biol., 26, 876–887, https://doi.org/10.1111/gcb.14905, 2020.

Krinner, G., Viovy, N., de Noblet-Ducoudré, N., Ogée, J., Polcher, J., Friedlingstein, P., Ciais, P., Sitch, S., and Prentice, I. C.: A dynamic global vegetation model for studies of the coupled atmosphere-biosphere system, Global Biogeochem. Cy., 19, 1–33, https://doi.org/10.1029/2003GB002199, 2005.

Lafleur, P. M., Roulet, N. T., Bubier, J. L., Frolking, S., and Moore, T. R.: Interannual variability in the peatland-atmosphere carbon dioxide exchange at an ombrotrophic bog, Global Biogeochem. Cy., 17, 1–14, https://doi.org/10.1029/2002gb001983, 2003.

Laine, A. M., Korrensalo, A., and Tuittila, E. S.: Plant functional traits play the second fiddle to plant functional types in explaining peatland CO_2 and CH_4 gas exchange, Sci. Total Environ., 834, 155352, https://doi.org/10.1016/j.scitotenv.2022.155352, 2022.

Li, T., Raivonen, M., Alekseychik, P., Aurela, M., Lohila, A., Zheng, X., Zhang, Q., Wang, G., Mammarella, I., Rinne, J., Yu, L., Xie, B., Vesala, T., and Zhang, W.: Importance of vegetation classes in modeling CH_4 emissions from boreal and subarctic wetlands in Finland, Sci. Total Environ., 572, 1111–1122, https://doi.org/10.1016/j.scitotenv.2016.08.020, 2016.

Lippmann, T. J. R., in 't Zandt, M. H., Van der Putten, N. N. L., Busschers, F. S., Hijma, M. P., van der Velden, P., de Groot, T., van Aalderen, Z., Meisel, O. H., Slomp, C. P., Niemann, H., Jetten, M. S. M., Dolman, H. A. J., and Welte, C. U.: Microbial activity, methane production, and carbon storage in Early Holocene North Sea peats, Biogeosciences, 18, 5491–5511, https://doi.org/10.5194/bg-18-5491-2021, 2021.

Lippmann, T. J. R. and van Huissteden, J.: Peatland-VU-NUCOM (PVN 1.0): A peatland GHG emissions model using dynamic plant functional types, Zenodo, https://doi.org/10.5281/zenodo.7701698, 2023.

Littleton, E. W., Harper, A. B., Vaughan, N. E., Oliver, R. J., Duran-Rojas, M. C., and Lenton, T. M.: JULES-BE: representation of bioenergy crops and harvesting in the Joint UK Land Environment Simulator vn5.1, Geosci. Model Dev., 13, 1123–1136, https://doi.org/10.5194/gmd-13-1123-2020, 2020.

Loisel, J., Gallego-Sala, A. V., Amesbury, M. J., Magnan, G., Anshari, G., Beilman, D. W., Benavides, J. C., Blewett, J., Camill, P., Charman, D. J., Chawchai, S., Hedgpeth, A., Kleinen, T., Korhola, A., Large, D., Mansilla, C. A., Müller, J., van Bellen, S., West, J. B., Yu, Z., Bubier, J. L., Garneau, M., Moore, T., Sannel, A. B., Page, S., Väliranta, M., Bechtold, M., Brovkin, V., Cole, L. E., Chanton, J. P., Christensen, T. R., Davies, M. A., De Vleeschouwer, F., Finkelstein, S. A., Frolking, S., Gałka, M., Gandois, L., Girkin, N., Harris, L. I., Heinemeyer, A., Hoyt, A. M., Jones, M. C., Joos, F., Juutinen, S., Kaiser, K., Lacourse, T., Lamentowicz, M., Larmola, T., Leifeld, J., Lohila, A., Milner, A. M., Minkkinen, K., Moss, P., Naafs, B. D., Nichols, J., O'Donnell, J., Payne, R., Philben, M., Piilo, S., Quillet, A., Ratnayake, A. S., Roland, T. P., Sjögersten, S., Sonnentag, O., Swindles, G. T., Swinnen, W., Talbot, J., Treat, C., Valach, A. C., and Wu, J.: Expert assessment of future vulnerability of the global peatland carbon sink, Nat. Clim. Change, 11, 70–77, https://doi.org/10.1038/s41558-020-00944-0, 2021.

Malmer, N., Albinsson, C., Svensson, B. M., and Wallén, B.: Interferences between Sphagnum and vascular plants: Effects on plant community structure and peat formation, Oikos, 100, 469–482, https://doi.org/10.1034/j.1600-0706.2003.12170.x, 2003.

Malmer, N., Johansson, T., Olsrud, M., and Christensen, T. R.: Vegetation, climatic changes and net carbon sequestration in a North-Scandinavian subarctic mire over 30 years, Glob. Change Biol., 11, 1895–1909, https://doi.org/10.1111/j.1365-2486.2005.01042.x, 2005.

Masson-Delmotte, V., Zhai, P., Pirani, A., Connors, S. L., Péan, C., Berger, S., Caud, N., Chen, Y., Goldfarb, L., Gomis, M. I., Huang, M., Leitzell, K., Lonnoy, E., Matthews, J. B. R., Maycock, T. K., Waterfield, T., Yelekçi, O., Yu, R., and Zhou, B. (Eds.): Climate Change 2021 – The Physical Science Basis, in: Climate Change 2021 – The Physical Science Basis Cambridge University Press, Cambridge, United Kingdom and New York, NY, USA, 34, F0003–F0003, https://doi.org/10.1017/9781009157896, 2021.

Mazzola, V., Perks, M. P., Smith, J., Yeluripati, J., and Xenakis, G.: Assessing soil carbon dioxide and methane fluxes from a Scots pine raised bog-edge-woodland, J. Environ. Manage., 302, 114061, https://doi.org/10.1016/j.jenvman.2021.114061, 2022.

Melillo, J. M., Steudler, P. A., Aber, J. D., Newkirk, K., Lux, H., Bowles, F. P., Catricala, C., Magill, A., Ahrens, T., and Morrisseau, S.: Soil warming and carbon-cycle feedbacks to the climate system, Science, 298, 2173–2176, https://doi.org/10.1126/science.1074153, 2002.

Melton, J. R., Wania, R., Hodson, E. L., Poulter, B., Ringeval, B., Spahni, R., Bohn, T., Avis, C. A., Beerling, D. J., Chen, G., Eliseev, A. V., Denisov, S. N., Hopcroft, P. O., Lettenmaier, D. P., Riley, W. J., Singarayer, J. S., Subin, Z. M., Tian, H., Zürcher, S., Brovkin, V., van Bodegom, P. M., Kleinen, T., Yu, Z. C.,

and Kaplan, J. O.: Present state of global wetland extent and wetland methane modelling: conclusions from a model inter-comparison project (WETCHIMP), Biogeosciences, 10, 753–788, https://doi.org/10.5194/bg-10-753-2013, 2013.

Metzger, C., Jansson, P.-E., Lohila, A., Aurela, M., Eickenscheidt, T., Belelli-Marchesini, L., Dinsmore, K. J., Drewer, J., van Huissteden, J., and Drösler, M.: CO_2 fluxes and ecosystem dynamics at five European treeless peatlands – merging data and process oriented modeling, Biogeosciences, 12, 125–146, https://doi.org/10.5194/bg-12-125-2015, 2015.

Mi, Y., van Huissteden, J., Parmentier, F. J. W., Gallagher, A., Budishchev, A., Berridge, C. T., and Dolman, A. J.: Improving a plot-scale methane emission model and its performance at a northeastern Siberian tundra site, Biogeosciences, 11, 3985–3999, https://doi.org/10.5194/bg-11-3985-2014, 2014.

Moore, T. R., Bubier, J. L., and Bledzki, L.: Litter decomposition in temperate peatland ecosystems: The effect of substrate and site, Ecosystems, 10, 949–963, https://doi.org/10.1007/s10021-007-9064-5, 2007.

Morin, T. H., Bohrer, G., Frasson, R. P., Naor-Azreli, L., Mesi, S., Stefanik, K. C., and Schäfer, K. V.: Environmental drivers of methane fluxes from an urban temperate wetland park, J. Geophys. Res.-Biogeo., 119, 2188–2208, https://doi.org/10.1002/2014JG002750, 2014a.

Morin, T. H., Bohrer, G., Naor-Azrieli, L., Mesi, S., Kenny, W. T., Mitsch, W. J., and Schäfer, K. V. R.: The seasonal and diurnal dynamics of methane flux at a created urban wetland, Ecol. Eng., 72, 74–83, https://doi.org/10.1016/j.ecoleng.2014.02.002, 2014b.

Morin, T. H., Bohrer, G., Stefanik, K. C., Rey-Sanchez, A. C., Matheny, A. M., and Mitsch, W. J.: Combining eddy-covariance and chamber measurements to determine the methane budget from a small, heterogeneous urban flood-plain wetland park, Agr. Forest Meteorol., 237-238, 160–170, https://doi.org/10.1016/j.agrformet.2017.01.022, 2017.

Muñoz-Sabater, J., Dutra, E., Agustí-Panareda, A., Albergel, C., Arduini, G., Balsamo, G., Boussetta, S., Choulga, M., Harrigan, S., Hersbach, H., Martens, B., Miralles, D. G., Piles, M., Rodríguez-Fernández, N. J., Zsoter, E., Buontempo, C., and Thépaut, J.-N.: ERA5-Land: a state-of-the-art global reanalysis dataset for land applications, Earth Syst. Sci. Data, 13, 4349–4383, https://doi.org/10.5194/essd-13-4349-2021, 2021.

Ostle, N. J., Smith, P., Fisher, R., Ian Woodward, F., Fisher, J. B., Smith, J. U., Galbraith, D., Levy, P., Meir, P., McNamara, N. P., and Bardgett, R. D.: Integrating plant-soil interactions into global carbon cycle models, J. Ecol., 97, 851–863, https://doi.org/10.1111/j.1365-2745.2009.01547.x, 2009.

Pangala, S. R., Moore, S., Hornibrook, E. R., and Gauci, V.: Trees are major conduits for methane egress from tropical forested wetlands, New Phytol., 197, 524–531, https://doi.org/10.1111/nph.12031, 2013.

Peltoniemi, K., Fritze, H., and Laiho, R.: Response of fungal and actinobacterial communities to water-level drawdown in boreal peatland sites, Soil Biol. Biochem., 41, 1902–1914, https://doi.org/10.1016/j.soilbio.2009.06.018, 2009.

Puma, M. J., Koster, R. D., and Cook, B. I.: Phenological versus meteorological controls on land-atmosphere water and carbon fluxes, J. Geophys. Res.-Biogeo., 118, 14–29, https://doi.org/10.1029/2012JG002088, 2013.

Saarnio, S., Wittenmayer, L., and Merbach, W.: Rhizospheric exudation of Eriophorum vaginatum L. – Potential link to methanogenesis, Plant Soil, 267, 343–355, https://doi.org/10.1007/s11104-005-0140-3, 2004.

Saleska, S. R., Shaw, M. R., Fischer, M. L., Dunne, J. A., Still, C. J., Holman, M. L., and Harte, J.: Plant community composition mediates both large transient decline and predicted long-term recovery of soil carbon under climate warming, Global Biogeochem. Cy., 16, 3-1–3-18, https://doi.org/10.1029/2001gb001573, 2002.

Schipper, L. A. and Reddy, K. R.: Determination of Methane Oxidation in the Rhizosphere of Sagittaria lancifolia Using Methyl Fluoride, Soil Sci. Soc. Am. J., 60, 611–616, https://doi.org/10.2136/sssaj1996.03615995006000020039x, 1996.

Schrier-Uijl, A. P., Kroon, P. S., Hendriks, D. M. D., Hensen, A., Van Huissteden, J., Berendse, F., and Veenendaal, E. M.: Agricultural peatlands: towards a greenhouse gas sink – a synthesis of a Dutch landscape study, Biogeosciences, 11, 4559–4576, https://doi.org/10.5194/bg-11-4559-2014, 2014.

Sitch, S., Smith, B., Prentice, I. C., Arneth, A., Bondeau, A., Cramer, W., Kaplan, J. O., Levis, S., Lucht, W., Sykes, M. T., Thonicke, K., and Venevsky, S.: Evaluation of ecosystem dynamics, plant geography and terrestrial carbon cycling in the LPJ dynamic global vegetation model, Glob. Change Biol., 9, 161–185, https://doi.org/10.1046/j.1365-2486.2003.00569.x, 2003.

Smith, B., Prentice, I. C., and Sykes, M. T.: Representation of vegetation dynamics in the modelling of terrestrial ecosystems: comparing two contrasting approaches within European climate space, Global Ecol. Biogeogr., 10, 621–637, https://doi.org/10.1046/j.1466-822x.2001.t01-1-00256.x, 2001.

Smithwick, E. A., Lucash, M. S., McCormack, M. L., and Sivandran, G.: Improving the representation of roots in terrestrial models, Ecol. Model., 291, 193–204, https://doi.org/10.1016/j.ecolmodel.2014.07.023, 2014.

Speckman, H. N., Frank, J. M., Bradford, J. B., Miles, B. L., Massman, W. J., Parton, W. J., and Ryan, M. G.: Forest ecosystem respiration estimated from eddy covariance and chamber measurements under high turbulence and substantial tree mortality from bark beetles, Glob. Change Biol., 21, 708–721, https://doi.org/10.1111/gcb.12731, 2015.

Strack, M., Waller, M. F., and Waddington, J. M.: Sedge succession and peatland methane dynamics: A potential feedback to climate change, Ecosystems, 9, 278–287, https://doi.org/10.1007/s10021-005-0070-1, 2006.

Ström, L., Mastepanov, M., and Christensen, T. R.: Species-specific Effects of Vascular Plants on Carbon Turnover and Methane Emissions from Wetlands, Biogeochemistry, 75, 65–82, https://doi.org/10.1007/s10533-004-6124-1, 2005.

Ström, L., Falk, J. M., Skov, K., Jackowicz-Korczynski, M., Mastepanov, M., Christensen, T. R., Lund, M., and Schmidt, N. M.: Controls of spatial and temporal variability in CH4 flux in a high arctic fen over three years, Biogeochemistry, 125, 21–35, https://doi.org/10.1007/s10533-015-0109-0, 2015.

Tiemeyer, B., Albiac Borraz, E., Augustin, J., Bechtold, M., Beetz, S., Beyer, C., Drosler, M., Ebli, M., Eickenscheidt, T., Fiedler, S., Forster, C., Freibauer, A., Giebels, M., Glatzel, S., Heinichen, J., Hoffmann, M., Hoper, H., Jurasinski, G., Leiber-Sauheitl, K., Peichl-Brak, M., Rosskopf, N., Sommer, M., and Zeitz, J.: High emissions of greenhouse gases from grasslands on peat

and other organic soils, Glob. Change Biol., 22, 4134–4149, https://doi.org/10.1111/gcb.13303, 2016.

Toet, S., Cornelissen, J. H., Aerts, R., Van Logtestijn, R. S., De Beus, M., and Stoevelaar, R.: Moss responses to elevated CO_2 and variation in hydrology in a temperate lowland peatland, Plant Ecol., 182, 27–40, https://doi.org/10.1007/s11258-005-9029-8, 2006.

Tramontana, G., Jung, M., Schwalm, C. R., Ichii, K., Camps-Valls, G., Ráduly, B., Reichstein, M., Arain, M. A., Cescatti, A., Kiely, G., Merbold, L., Serrano-Ortiz, P., Sickert, S., Wolf, S., and Papale, D.: Predicting carbon dioxide and energy fluxes across global FLUXNET sites with regression algorithms, Biogeosciences, 13, 4291–4313, https://doi.org/10.5194/bg-13-4291-2016, 2016.

Van den Hoof, C., Hanert, E., and Vidale, P. L.: Simulating dynamic crop growth with an adapted land surface model – JULES-SUCROS: Model development and validation, Agr. Forest Meteorol., 151, 137–153, https://doi.org/10.1016/j.agrformet.2010.09.011, 2011.

van Geel, B., Bos, J. M., and Pals, J. P.: Archaeological and palaeoecological aspects of a medieval house terp in a reclaimed raiseg bog area in North Holland, Ber. Rijksd. Oudheidkd. Bodemonderz, 33, 419–444, 1983.

van Huissteden, J., van den Bos, R., and Marticorena Alvarez, I.: Modelling the effect of water-table management on CO_2 and CH_4 fluxes from peat soils, Neth. J. Geosci., 85, 3–18, https://doi.org/10.1017/S0016774600021399, 2006.

van Huissteden, J., Petrescu, A. M. R., Hendriks, D. M. D., and Rebel, K. T.: Sensitivity analysis of a wetland methane emission model based on temperate and arctic wetland sites, Biogeosciences, 6, 3035–3051, https://doi.org/10.5194/bg-6-3035-2009, 2009.

Waddington, J. M. and Roulet, N. T.: Carbon balance of a Boreal patterned peatland, Glob. Change Biol., 6, 87–97, https://doi.org/10.1046/j.1365-2486.2000.00283.x, 2000.

Waldo, N. B., Hunt, B. K., Fadely, E. C., Moran, J. J., and Neumann, R. B.: Plant root exudates increase methane emissions through direct and indirect pathways, Biogeochemistry, 145, 213–234, https://doi.org/10.1007/s10533-019-00600-6, 2019.

Walter, B. P. and Heimann, M.: A process-based, climate-sensitive model to derive methane emissions from natural wetlands: Application to five wetland sites, sensitivity to model parameters, and climate, Global Biogeochem. Cy., 14, 745–765, https://doi.org/10.1029/1999GB001204, 2000.

Wania, R., Ross, I., and Prentice, I. C.: Implementation and evaluation of a new methane model within a dynamic global vegetation model: LPJ-WHyMe v1.3.1, Geosci. Model Dev., 3, 565–584, https://doi.org/10.5194/gmd-3-565-2010, 2010.

Wania, R., Melton, J. R., Hodson, E. L., Poulter, B., Ringeval, B., Spahni, R., Bohn, T., Avis, C. A., Chen, G., Eliseev, A. V., Hopcroft, P. O., Riley, W. J., Subin, Z. M., Tian, H., van Bodegom, P. M., Kleinen, T., Yu, Z. C., Singarayer, J. S., Zürcher, S., Lettenmaier, D. P., Beerling, D. J., Denisov, S. N., Prigent, C., Papa, F., and Kaplan, J. O.: Present state of global wetland extent and wetland methane modelling: methodology of a model inter-comparison project (WETCHIMP), Geosci. Model Dev., 6, 617–641, https://doi.org/10.5194/gmd-6-617-2013, 2013.

WGI: Climate Change 2021 The Physical Science Basis WGI, vol. 34, John Wiley and Sons Ltd., ISBN 9781009157896, 2021.

Whipps, J. M.: Carbon economy, The rhizosphere, 59–97, 1990.

Wu, Y. and Blodau, C.: PEATBOG: a biogeochemical model for analyzing coupled carbon and nitrogen dynamics in northern peatlands, Geosci. Model Dev., 6, 1173–1207, https://doi.org/10.5194/gmd-6-1173-2013, 2013.

WWu, Y., Verseghy, D. L., and Melton, J. R.: Integrating peatlands into the coupled Canadian Land Surface Scheme (CLASS) v3.6 and the Canadian Terrestrial Ecosystem Model (CTEM) v2.0, Geosci. Model Dev., 9, 2639–2663, https://doi.org/10.5194/gmd-9-2639-2016, 2016.

Wullschleger, S. D., Epstein, H. E., Box, E. O., Euskirchen, E. S., Goswami, S., Iversen, C. M., Kattge, J., Norby, R. J., Van Bodegom, P. M., and Xu, X.: Plant functional types in Earth system models: Past experiences and future directions for application of dynamic vegetation models in high-latitude ecosystems, Ann. Bot., 114, 1–16, https://doi.org/10.1093/aob/mcu077, 2014.

Yrjälä, K., Tuomivirta, T., Juottonen, H., Putkinen, A., Lappi, K., Tuittila, E. S., Penttilä, T., Minkkinen, K., Laine, J., Peltoniemi, K., and Fritze, H.: CH4 production and oxidation processes in a boreal fen ecosystem after long-term water table drawdown, Glob. Change Biol., 17, 1311–1320, https://doi.org/10.1111/j.1365-2486.2010.02290.x, 2011.

Yu, Z., Loisel, J., Brosseau, D. P., Beilman, D. W., and Hunt, S. J.: Global peatland dynamics since the Last Glacial Maximum, Geophys. Res. Lett., 37, 1–5, https://doi.org/10.1029/2010GL043584, 2010.

Zeng, X.: Global Vegetation Root Distribution for Land Modeling, J. Hydrometeorol., 2, 525–530, https://doi.org/10.1175/1525-7541(2001)002<0525:gvrdfl>2.0.co;2, 2001.

Zhao, J., Lange, H., and Meissner, H.: Gap-filling continuously-measured soil respiration data: A highlight of time-series-based methods, Agr. Forest Meteorol., 285–286, 107912, https://doi.org/10.1016/j.agrformet.2020.107912, 2020.